Source controls on mineralisation: Regional geology and magmatic evolution of Fiji

Rose Clarke [a],[*], Daniel Smith [a], Jonathan Naden [b]

[a] *University of Leicester, UK*
[b] *British Geological Survey, UK*

ARTICLE INFO

ABSTRACT

There is a well-established link between world-class gold telluride mineral deposits and alkalic magmatic host rocks, often emplaced post-subduction in arc terranes. Fiji is home to two such deposits, and provides an ideal location to study the relationship between the alkalic (shoshonitic) host rocks, their geodynamic context, and potential roles in metal enrichment. A total of 93 new geochemical analyses of magmatic rocks from across Fiji are presented, alongside detailed petrography and mineralogy and a new compilation of literature data. Despite relatively similar mineralogy across *syn-* and post-subduction samples, there are geochemical differences between them, with the latter displaying elevated concentrations of Ba (<2137 ppm), Rb (<218 ppm), Sr (<2648 ppm) and K_2O (<10.18 wt%), and depletions in Nb and Ta. Multi-element trends suggest exaggerations of 'typical' arc patterns in post-subduction shoshonites. Geochemical data suggest that whilst the fluxing of fluids and sediment melts from a subducted slab may play a role in producing the distinctive post-subduction magmas, they are likely insufficient to drive such strong trends. Instead, biotite or possibly phlogopite in the lithosphere are suggested as being a key 'ingredient'. Earlier subduction can modify the lithosphere through the addition of hydrous phases, both by metasomatism of the lithospheric mantle, or by the formation of residual minerals during fractional crystallisation. Remelting of these phases could liberate trace elements and metals. Biotite in particular could facilitate some of the observed large ion lithophile elements (LILE) enrichments and the alkali-rich (potassic) nature of the magmas.

1. Introduction

Alkaline rocks are uncommon in arc settings but are an important host for economic mineralisation. Some of the world's largest gold deposits are associated with alkaline rocks (Pals and Spry, 2003), and in many cases show features which distinguish them from calc-alkaline associated mineral deposits, including total metal endowment, abundant tellurides, and paucity of acid-related hydrothermal alteration (Jensen and Barton, 2000; Smith et al., 2017). Porphyry and epithermal mineralisation in arcs is often hosted in the abundant calc-alkaline compositions that dominate during subduction (du Bray, 2017); alkaline arc magmas are much less common, and are often post-subduction in timing (Ciobanu et al., 2006; Jensen and Barton, 2000; Kelley and Spry, 2016; Sillitoe, 2002).

Despite the associations between post-subduction tectonics, alkaline magmatism, and gold (telluride) mineralisation, the source of and mechanisms for metal enrichment remain uncertain. Richards (2009)

proposed a model that outlined the importance of the transition from subduction to post-subduction regimes. This shift allows later magmas to recycle metal-rich material in the lithosphere, generated during earlier subduction. Remelting of metasomatised mantle or hydrous, ultramafic cumulates is suggested to produce the alkaline magmatism and to remobilise Au, and presumably Te too (Holwell et al., 2019). Alternative models for the association between alkaline magmas and mineralisation include sediment inputs during subduction. Tellurium may be enriched in deep-marine sediments. Thus, it has been suggested that Te may be released during subduction and transferred to the mantle wedge (Jensen and Barton, 2000), with siliciclastic detrital phases contributing alkali elements (Plank and Langmuir, 1998). The altered, hydrated part of the ocean crust (and possibly serpentinised mantle) will also carry a cargo of elements into the subduction zone, possibly elevating concentrations.

The Fijian island of Viti Levu is host to alkaline, potassic magmas that were emplaced in and erupted from a series of volcano-intrusive centres

during late-stage arc activity, throughout a period of extension and rotation of the island away from the main arc. These post-subduction centres host gold-telluride mineralisation, including the Tuvatu deposit (under exploration) and the Vatukoula Gold Mines (also known as the Emperor Gold Deposit), which have produced ~7 Moz of Au since 1933. In this study, we use Fiji and particularly Viti Levu as a study area to examine the role of melt sources and crustal processes in the formation of alkaline magmas and gold telluride mineralisation. These are placed into the context of the geological evolution of Fiji and Viti Levu, to better examine the role that earlier subduction might play in modifying the mantle or lithosphere before post-subduction magmatism. Alkaline magmas in arc settings, including those associated with mineralisation, may be a result of low degree partial mantle (asthenosphere) melting (Kelley and Ludington, 2002; Richards et al., 1990), melting of meta-somatised lithospheric mantle (Grondahl and Zajacz, 2017; Holwell et al., 2019), remelting of cumulates (Hou et al., 2015; Lee and Tang, 2020; Richards, 2009; Richards, 2011), or combinations of these processes. Cumulates (sensu *lato*; we include all residues of magmatic differentiation, including those produced by reaction-replacement processes in lithospheric mushes e.g., Smith, 2014) are considered an important reservoir for sulphides and metals fractionated during subduction magmatism (Core et al., 2006; Holwell et al., 2022; Lee and Tang, 2020), and their partial melting or assimilation can produce alkaline magmas (Reubi and Blundy, 2008; Sorbadere et al., 2013).

Previous petrogenetic studies conducted in Fiji have been done on specific volcanic centres (e.g., Tavua: (Rogers and Setterfield, 1994)); or suites of magmatic rocks (OIBs: (Gill and Whelan, 1989b); or shoshonites: (Gill and Whelan, 1989a)), but rarely consider them in the context of the preceding magmatism and metasomatism. Studies into the mineralised centres across Fiji such as Vatukoula / Emperor (Anderson and Eaton, 1990) or Tuvatu (Scherbarth and Spry, 2006) have provided little detail on the genesis of host magmas, despite the magmas being considered as the source of mineralisation.

This study integrates new and legacy whole-rock geochemical data from across Fiji, combining nationwide datasets from Gill (1987), Gill and Whelan (1989a); Gill and Whelan (1989b); detailed studies of specific igneous centres including Tavua (Rogers and Setterfield, 1994); mineral deposits including Vatukoula (Anderson and Eaton, 1990) and Tuvatu (Scherbarth and Spry, 2006) and new samples. New data includes 93 geochemical analyses of major and trace elements. Samples were collected with a focus on alkaline centres across Viti Levu which host mineralisation, including Vatukoula and the lesser-studied Tuvatu. Our aim is to use petrography and geochemistry to constrain the sources of melts for mineralised alkaline magmatic systems in Fiji and advance our broader understanding of this class of mineralisation.

2. Geological overview of Fiji

2.1. Background

At present, the Fijian islands sit on the Fiji Platform (FP), a block of anomalously thick former arc lithosphere situated at the transfer/ transform offset between two opposing subduction zones: the Tonga Arc, where the Pacific Plate is subducting beneath the Indo-Australian Plate, and the Vanuatu Arc, which has the opposite polarity. To accommodate divergence between the two subduction zones, extensive spreading and transform-faulting has been ongoing since ~10 Ma (Begg and Gray, 2002; Hamburger and Isacks, 1988). The Fijian islands record a complex history of subduction initiation, cessation, extension, rifting and basin formation, shortening and basin inversion, over a ~ 40My period (Fig. 1). We divide the geological history of Fiji into three phases: *syn*-subduction, transitional and post-subduction, and a later remnant-arc phase (Fig. 2). A simplified geological map of Viti Levu showing the main outcropping groups mentioned is shown in Fig. 3.

2.2. Syn-subduction phase

Syn-subduction Phase lithologies are related to magmatic activity along the Vitiaz Arc prior to ~10 Ma, which involved subduction of the Pacific Plate beneath the Indo-Australian Plate. The Yavuna Group are the oldest rocks in Fiji and represent proto-arc activity. This group consists of lavas and intrusives of tholeiitic and boninitic composition and are of Late Eocene to Early Oligocene age. The Wainimala Group sits unconformably above the Yavuna Group, forming between 32 and 13 Ma (Hathway, 1993). This group is the best-exposed *syn*-subduction unit on Viti Levu and displays increasingly calc-alkaline arc volcanism (Hathway, 1994); older rocks are dominated by andesites and andesitic volcaniclastics with some limestones, whilst younger rocks include volcanic conglomerates, pillow lavas, and breccias (Rodda, 1967).

The Colo 'Orogeny' (12–7 Ma) was related to termination of Vitiaz subduction due to collision with thick lithosphere of the Melanesian Border Plateau, and more regionally, the Ontong Java Plateau (Begg and Gray, 2002). The Colo Orogeny produced large-scale folding and faulting of the Wainimala Group, and intrusion of the Colo Plutonic Suite (Begg and Gray, 2002; Gill, 1987).

The timing of subduction and the Syn-subduction Phase is well constrained, with major groups bounded by unconformities and dated using K—Ar (Wharton et al., 1995) and biostratigraphy (Hathway, 1994). Whilst K—Ar dating is now considered a limited method, dates agree with biostratigraphy. All new subduction-age samples for this study were collected from Viti Levu and are from the Wainimala Group, including the Nadele Breccia which is a member of the Group (Scherbarth and Spry, 2006). Literature data comes from Suva Group, the Kawa Formation, the Yavuna Dyke, and samples from across the wider arc including the Lau Volcanic Group (Table 1).

2.3. Transitional and post-subduction phase

Somewhere between 10 and 7.5 Ma, active subduction beneath Fiji ceased due to the oblique collision of the Ontong-Java Plateau to the northwest and the Melanesian Border Plateau immediately north of Fiji (Begg and Gray, 2002). Collision resulted in the ca 12–7 Ma Colo Orogeny. This triggered a subduction flip, initiating the east-dipping Vanuatu subduction zone north of Fiji. A diffuse east-west left-lateral transform system then developed either side of the FP to accommodate divergence of the Vanuatu (east-dipping subduction) and Tonga-Kermadec (west-dipping subduction) trenches, broadly simultaneous with SW-NE extension and development of several broadly linear NW-trending sedimentary basins across the Fiji Platform (Hathway, 1993). The North Fiji Basin opened as a consequence of this divergence from ca 7 Ma, accompanied by an initial component of anticlockwise rotation of the Fijian Platform (Begg and Gray, 2002; Hathway, 1993; Rahiman and Pettinga, 2008).

The North Fiji Basin's 'incipient rifting stage' may have commenced as early as 8 Ma and continued between 5.5 and 3 Ma. During later stages, current spreading patterns initiated as the Lau Ridge split and the Lau Basin opened (Hergt and Woodhead, 2007) – a final severance of Fiji from the Vitiaz Arc system (Stratford and Rodda, 2000).

During the rotation of the Fiji Platform, between ~5 and 4.6 Ma, the Fiji Platform became subject to N-S compression (Begg and Gray, 2002), basin inversion (Hathway, 1993), crustal thickening (Chen et al., 2019), and declining volcanic activity in Viti Levu, with little to no activity after 3 Ma.

From Late Miocene through to Early Pliocene, shoshonitic lavas erupted across Fiji (Gill & Whelan, 1989a), and were particularly focused within the linear post-collisional extensional basins (Hathway, 1993). The oldest are the Sabeto Volcanics of the Koroimavua Volcanic Group at 5.35 Ma (Hathway, 1993), and Ba Volcanic Group at ca. 5 Ma (Setterfield et al., 1992), which formed closest to the rifting margin (Gill & Whelan, 1989a). Shoshonites (also inclusive of the Ba Volcanic Group) are associated with mineralisation across Fiji. The term shoshonite is
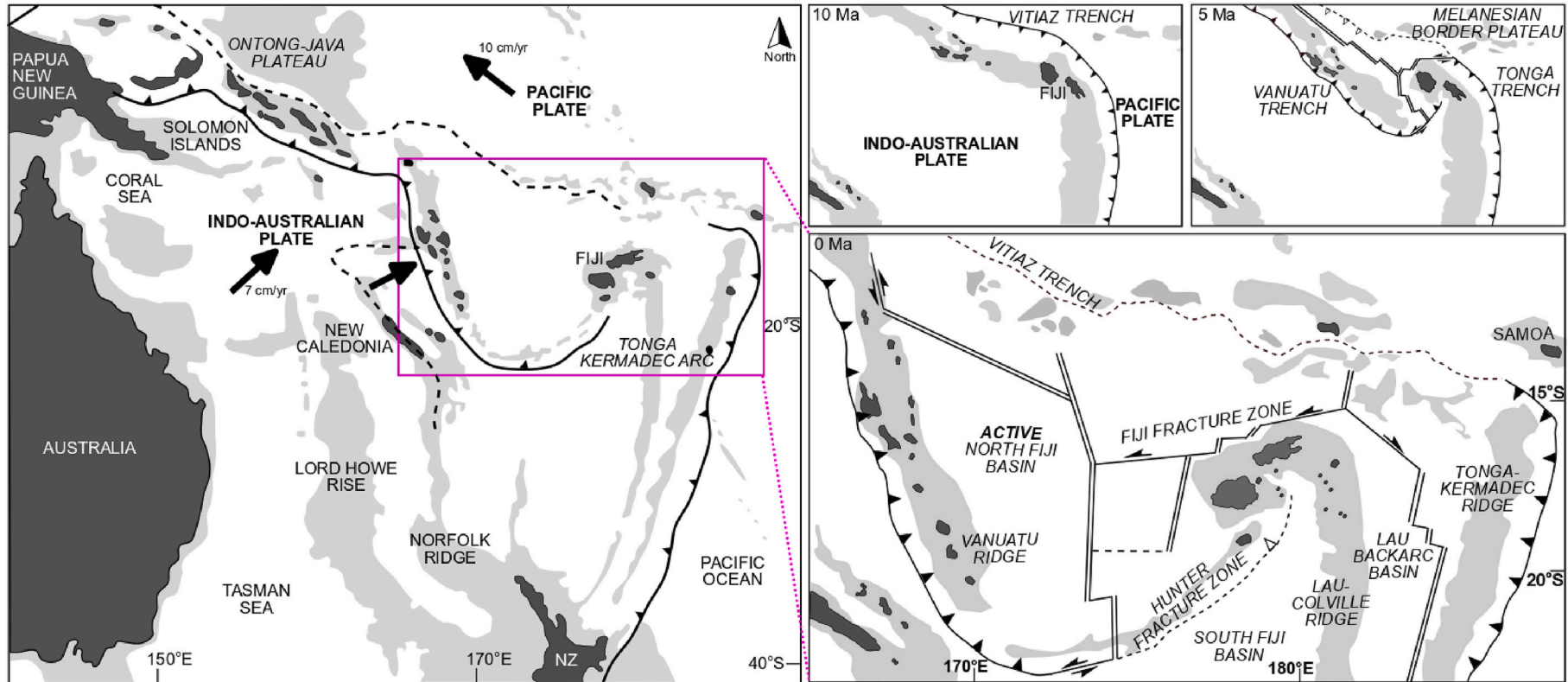
Fig. 1. Map showing the current tectonic setting of the southwest-Pacific, along with a more detailed view of the geodynamics of Fiji (Begg and Gray, 2002) during active subduction at 10 Ma, equivalent to *syn*-subduction phase; collision and basin initiation at approximately 5 Ma, representative of the transitional and post-subduction phase; and the present-day configuration, consistent with the latter stages of the later remnant arc phase used in this study. Active arcs are shown as solid lines with arrow marks on overriding plate; inactive arcs are shown as dashed lines; spreading ridges are shown as double lines; arrows show relative plate motions (Petterson et al., 1999). Light gray areas illustrate the bathymetric ~2000 m contour. Note no coordinates are used for earlier reconstructions as they are not well constrained.
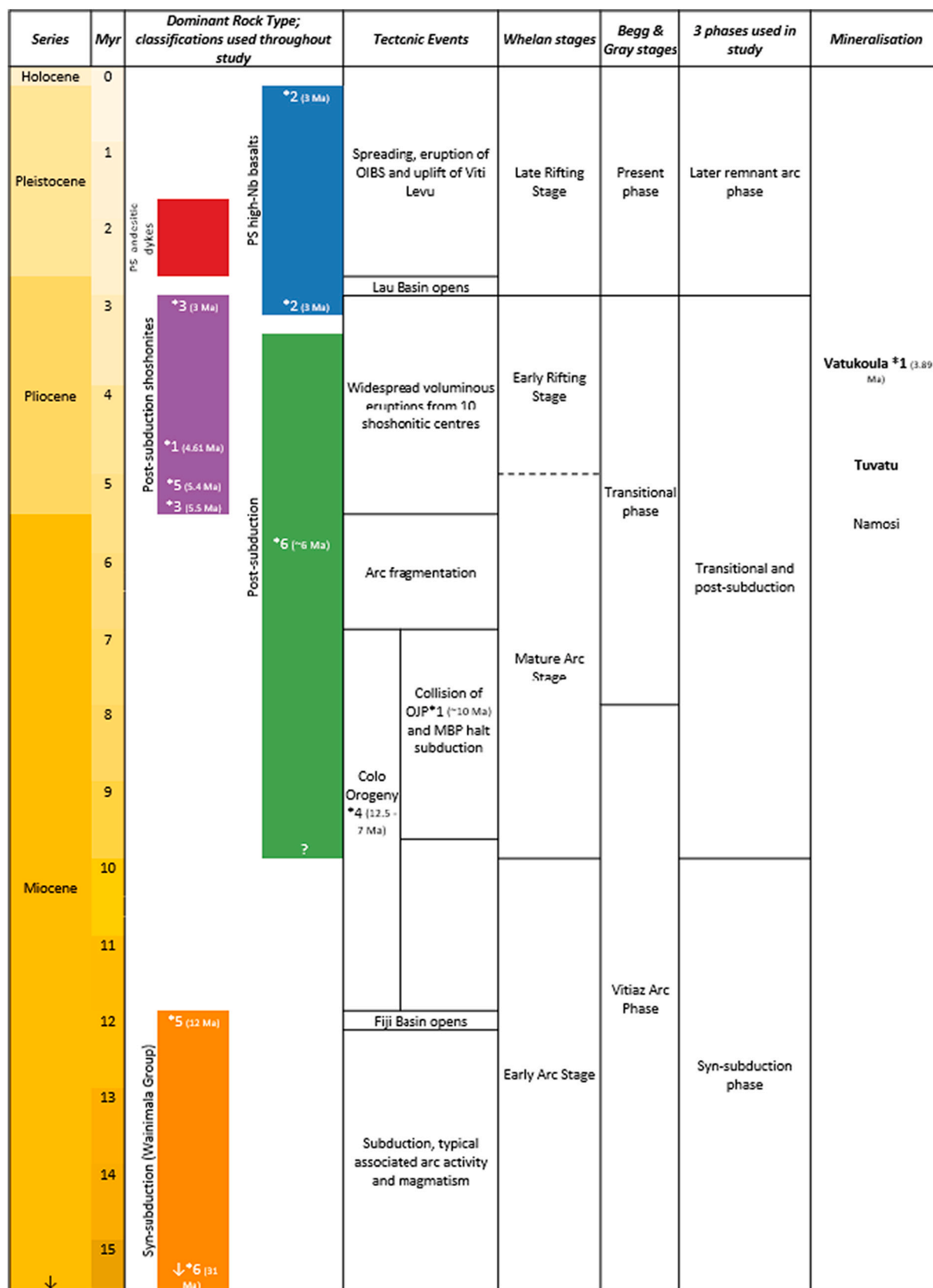
Fig. 2. The tectonic framework as referred to throughout this study, highlighting the classification used throughout, the major tectonic events, Whelan stages which refer to those proposed by Whelan et al. (1985) and period of mineralisation. Asterisks show where specific dates have been given elsewhere: 1 = Begg and Gray (2002), 2 = Gill and Whelan (1989a), 3 = Gill and Whelan (1989b), 4 = Hathway, 1993, 5 = Scherbarth and Spry (2006), and 6 = Stratford and Rodda (2000).
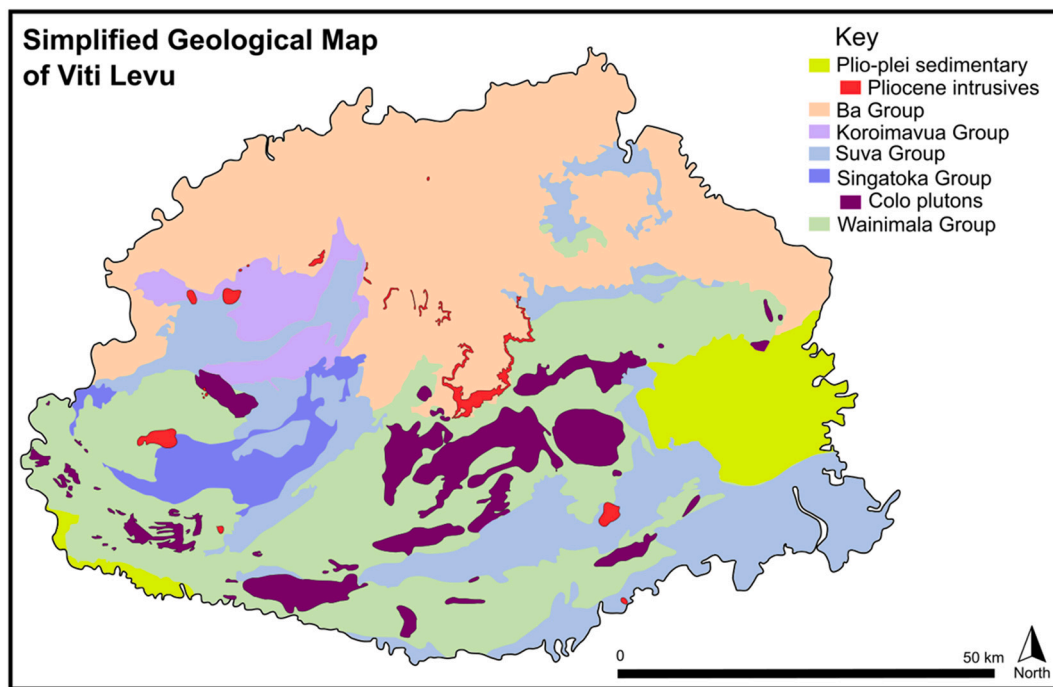
Fig. 3. Simplified geological map of Viti Levu.

Table 1

Information on the included datasets used throughout study, including the location of the samples, the arc stage they come from and the literature in which they were published.

Location	Arc stage	Reference
Lau and Viti Levu	Syn-subduction; Transitional	Gill (1987)
Taveuni, Vanua Levu	Pot-subduction high-Nb basalts	Gill and Whelan (1989a)
Viti Levu, Vanua Levu and Lau	Post-subduction; post-subduction shoshonites	Gill and Whelan (1989b)
Lau arc	Syn-subduction; Transitional	Cole (1990)
Viti Levu: Tavua	Post-subduction shoshonites	Rogers and Setterfield (1994)
Yavuna	Syn-subduction	Wharton (1994)
Viti Levu: Tuvatu	Post-subduction shoshonites, post-subduction andesitic dykes	Spry and Scherbarth (2006)
'Eau and Lau	Syn-subduction	Hergt and Woodhead (2007)
Astrolabe Islands, Vatu-i-Cake, Viti Levu	Post-subduction shoshonites	Leslie et al. (2009)

used generally to encompass samples in the shoshonite series in line with previous work (Leslie et al., 2009). Most have been dated, forming between 5.5 and 3 Ma and as potassic equivalents of trachybasalts to trachyandesites are alkaline lithologies. Volcanic centres are structurally controlled, as is highlighted in Fig. 4. Examples of shoshonitic centres include Tavua (host to Vatukoula Gold Mines / Emperor), Navilawa (host to Tuvatu), Sabeto, Fadis, and Raki-Raki. Literature data is included from Lomaiviti. Data from the "Astrolabe Islands" (properly the Kadavu Group and Great Astrolabe Reef) are not included despite being considered as equivalent in other studies (Leslie et al., 2009), due to its young age (3 Ma) and occurrence outside of the Fiji Platform.

All other igneous rocks formed between 10 and 3 Ma are grouped here as 'transitional'. Multiple examples across the arc include calc-alkaline rocks; the Suva Group; the Mago Volcanic Group (MVG); and the 6–3 Ma Namosi Andesite (Gill, 1987). Many are contemporaneous with post-subduction shoshonites (Gill & Whelan, 1989). This, along with an unconformable relationship with the Wainimala Group, are

considered to sufficiently justify the grouping with the post-subduction rocks within the context of this study.

2.4. Later phase

Post 3.5–3 Ma, arc-like volcanism in Fiji ceased, and extensive anticlockwise rotation ended abruptly (Taylor et al., 2000) as the remnant-arc transitioned to a maturing transform-zone bounded by sinistral faulting along the Fiji Fracture Zone and Hunter Fracture Zone (Hamburger and Isacks, 1988; Rahiman and Pettinga, 2008). The Lau and North Fiji Basins both experienced seismicity and volcanism. Micro-earthquakes around Viti Levu suggest Fiji is under the same stress field as the deforming basins, indicating that the Fiji platform is not a stable microplate or landmass (Hamburger and Isacks, 1988).

The youngest magmatic rocks of Fiji are the post-subduction high-Nb basalts of the 'late-rifting stage' of Whelan et al. (1985). Although none are found on Viti Levu, they are present on the island of Vatu-i-Ra, <30 km offshore, and on Vanua Levu. They erupted during late rifting and have been characterised by TiO_2 contents >1.5 wt%, and Nb/La ratios >1 at MgO >8 wt%. The most recent volcanism in the basins surrounding Fiji reflect a change in alkalic volcanism from shoshonite to OIB in the Koro Sea and Lau regions (Leslie et al., 2009). To address late-stage volcanism on Viti Levu, Forsythe et al. (2019) consider basaltic–andesite 'dike' data from Tuvatu (Scherbarth and Spry, 2006) to be useful for comparative purposes. These have not been dated but are stratigraphically younger than the post-subduction alkaline volcanism and share some affinities to the post-subduction high-Nb basalts. The same data has been used for similar purposes here and are classified as 'post-subduction andesitic dykes'.

2.5. Regional mineralisation

Mining of Au-Ag-(Te) ores has historically occurred throughout Fiji, from large deposits such as Vatukoula / Emperor, to minor historical production at Mistry and Vunda (sic.) (Colley and Greenbaum, 1980). These and other important Au prospects such as Mt. Kasi and Tuvatu lie along the >250 km Viti Levu Lineament (Begg and Gray, 2002; Gill & Whelan, 1989), sometimes referred to as Fiji's Mineralised Gold Belt
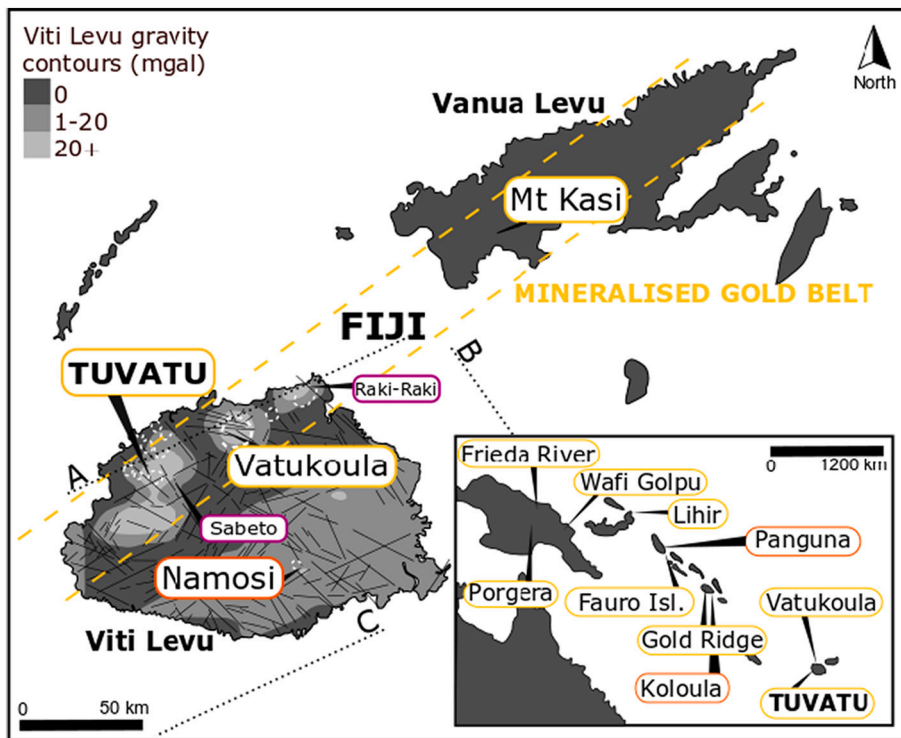
Fig. 4. Map showing the major gold and copper-gold deposits in Fiji, and throughout the southwest Pacific (inset: data from Holm et al., (2019)). Gravity anomaly data for Viti Levu is shown in gray scale with the key in the top left corner. Gold dashed lines show the Mineralised Gold Belt. Rahiman and Pettinga (2008) interpreted major faults, shown as thin black lines; three lineaments associated with shoshonites are shown as dashed lines labelled A-C in accordance with Gill and Whelan (1989b). Calderas on Viti Levu are dashed white lines and highlight the association of deposits with calderas. Gold deposits are in gold, gold prospects hosted in post-subduction calderas purple and porphyry copper-gold orange. (For interpretation of the references to colour in this figure legend, the reader is referred to the web version of this article.)

(Fig. 4). The porphyry copper deposit Namosi does not lie along the lineament but is worth noting given its size (1.2 Mt. Cu and 4.6 MOz Au resources), similar age, and proximity.

Previous regional gravity surveys of Fiji show strong anomalies correlating to four volcanic centres hosting mineralisation including Tuvatu and Vatukoula (Forsythe et al., 2019), illustrated on Fig. 4. All centres include alkaline calderas aged between 6 and 3 Ma and are associated with plate reconfiguration. At both Tuvatu and Vatukoula the alkaline rocks are assumed to be the source of metals (Scherbarth and Spry, 2006), and mineralising fluids at Vatukoula determined as being magmatic (Ahmad, 1987). Mineralisation at Tuvatu has not been accurately dated, but the age of mineralisation at Vatukoula is 3.89 Ma, based on Ar—Ar dating (Begg and Gray, 2002).

Three lineaments, A, B and C in Fig. 2 (Gill & Whelan, 1989), are believed to have controlled distribution of volcanic centres on the Fiji Platform, with northeast-trending fault zone 'A', commonly known as the Viti Levu Lineament, controlling shoshonitic centres across Viti Levu (Anderson and Eaton, 1990). Whilst the deep-seated fault system is observable by remote sensing imagery (Rahiman and Pettinga, 2008), its nature is not unanimously agreed (Hamburger and Isacks, 1988). Association of mineralisation with deep-seated fault systems is prevalent across the circum-Pacific region, where Au-porphyry and -epithermal systems are proposed to have been emplaced/controlled by faults (Sillitoe, 1997).

2.6. Sampling and analytical methods

2.6.1. Sampling methods

2.6.1.1. Direct sampling methods. Field seasons were conducted in 2017 and 2019. During both campaigns, samples from alkaline igneous complexes and other major volcanic groups from across Viti Levu were collected. Tropical weathering, typical of Pacific islands, makes many outcrops unsuitable for analytical work, hence most subduction-aged samples are from beaches or stream-cut exposures, and most post-subduction samples are from drill cores from various sites of gold

exploration projects; samples analysed in this study were chosen based on having little to no visible alteration or hydrothermal veining.

2.6.1.2. Literature data. Data was drawn from the literature to facilitate an arc-scale compilation. GEOROC was used to obtain a dataset. Samples were used where they were appropriately dated, had corresponding whole rock data, and level of alteration was low enough for the samples to be considered fresh. Only data published in peer-reviewed literature was included so that values could be cross-checked, and their suitability confirmed. The sources of major and trace element data incorporated in magmatic datasets are shown in Table 1.

2.7. Analytical methods

2.7.1. Petrography

A detailed petrographical study was conducted on 23 polished thin sections, all of which were produced from samples collected in 2019 and have corresponding geochemical analyses. Modal mineralogy was calculated using a Pelcon point counter. This was supplemented with thin sections produced from the 2017 field season.

2.7.2. X-ray fluorescence (XRF)

102 samples were analysed by XRF for both major and trace elements. Weathered surfaces were removed. Samples were coarsely crushed with a hardened steel press and powdered using agate planetary mills at the University of Leicester. Major elements were determined on fused glass beads prepared using a lithium tetraborate flux (sample to flux ratio 1:5) and trace elements on 32 mm diameter pressed powder pellets prepared using a small quantity of Moviol 8–88 binding agent. Analyses were conducted on a PANalytical Axios Advanced XRF spectrometer at the University of Leicester. Loss-on-ignition (LOI) values were determined for all samples from powders dried overnight at 105 °C, then ignited at 950 °C for 1 h, with values ranging from 0.09% to 9.72%. Data on accuracy and precision can be found in Appendix 1.

2.7.3. Inductively coupled plasma mass spectrometry (ICP-MS)

Ninety-eight samples were analysed at the University of Leicester for a range of trace elements including REE, using inductively coupled plasma mass spectrometry (ICP-MS). Samples collected in 2017 were prepared via digestion of fusion beads already made for the XRF, whilst those collected in 2019 were prepared via HNO_3, HF, and HCl acid digestion of milled powders to a 1000 x dilution. Some samples from 2017 were re-run along with the 2019 samples to ensure comparability. All solutions were spiked with a 100 mL of Rh/Ir and analysed using a ThermoScientific ICAP-Qc quadrupole ICP-MS attached to a Cetac ASX-520 Autosampler. Data on accuracy and precision can be found in Appendix 1.

Where data were collected for an element using both XRF and ICP-MS (Ba, Ce, Cs, La, Nb, Nd, Pb, Th, U, Y and Zr) data from only one method was used per element with the method chosen on an individual basis. This was done via assessing relative standard deviation and reference material traces with concentrations similar to those expected in the samples. Those used from XRF include Ba, Ce, Cs, Pb, Y and Zr; although Ce is usually overestimated by XRF, ICP consistently measures even higher values. Those used from ICP include La, Nb, Nd, Th, and U. Whilst XRF is usually preferable for Nb, relative standard deviation was lower for ICP-MS reference material.

2.8. Mineralogy and petrography

Due to the tropical climate in Fiji, petrography is sometimes made difficult due to alteration and weathering. For instance: feldspars are generally clouded, groundmass is occasionally heavily oxidised, and, where present, olivines are serpentinised.

2.8.1. Syn-subduction phase

Syn-subduction magmatic rocks from across Fiji studied petrologically here include gabbros, basalts, and andesites, and the volcaniclastic Nadele Breccia, all part of the Wainimala Group. Alteration is difficult to quantify in the Nadele Breccia due to its nature, which can be seen in Fig. 5 (a), where clasts of fine-grained (<1 mm) volcanic material reside in a crystalline matrix. Clasts have differing compositions and textures, however in Fig. 5(b) it is illustrated that feldspars, mainly plagioclase,
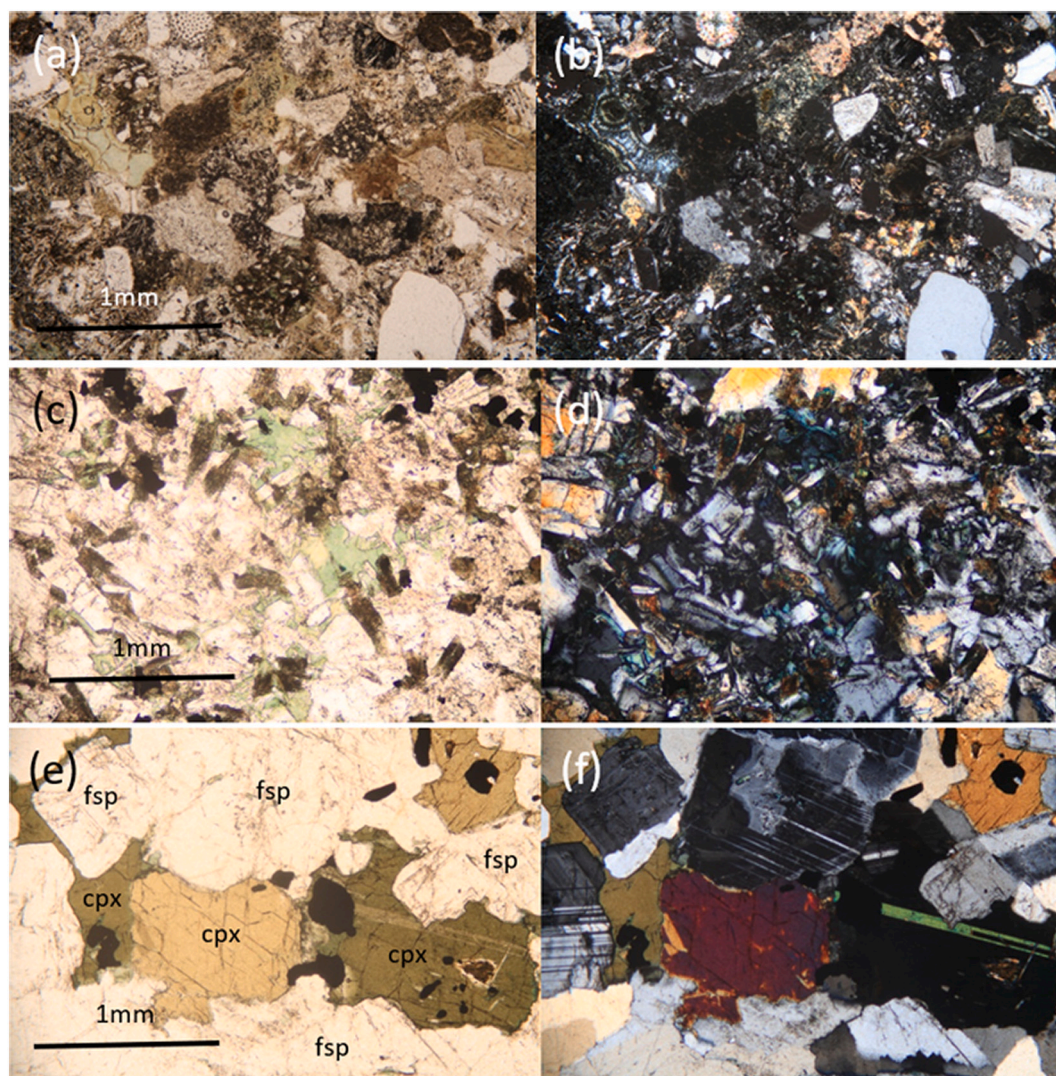
Fig. 5. Thin sections of *syn*-subduction rocks, all using transmitted light, left-hand image plane-polarised light and right-hand image cross-polarised light of the same view. FOV 3 mm across, scale bars shown on image. Minerals labelled according to abbreviations in table. (a) and (b) show the Nadele Breccia, with various clasts made up of fine-grained igneous material, green alteration minerals, clays, and feldspars. Both samples in (c)-(f) show rocks of the same age and mineralogy but with different textures. (c) and (d) show fine-grained rocks from Koroviolou Village, with poikilitic feldspars and minor chlorite alteration. (e) and (f) show equivalent medium-grained material, where the relatively fresh feldspars (fsp) and clinopyroxenes (cpx) can be more easily identified. Minor opaque phases are all oxides. (For interpretation of the references to colour in this figure legend, the reader is referred to the web version of this article.)

dominate both clasts and the groundmass, and alteration minerals including adularia, actinolite, chlorite, epidote and sericite are all present. Clay alteration makes mafic minerals difficult to identify. Volcanic samples have a similar mineralogy to the Nadele Breccia, as seen in Fig. 5 (c) through (f). Crystal size varies significantly across samples, from <1 mm to 3 mm. All samples contain numerous feldspars and pyroxenes that are dominated by clinopyroxene. No fresh olivine is observed in any thin section; some andesitic samples contain minor biotite and one showed primary amphibole, though neither of these are found in cumulate/phaneritic samples. Alteration minerals including sericite, chlorite, epidote, actinolite, and oxides are also abundant.

2.8.2. Transitional phase

Transitional rocks of the Suva Group have a sericitised fine-grained feldspar groundmass. Phenocrysts include plagioclase laths with altered centres; tabular and basal biotite altered to green chlorite; abundant euhedral clinopyroxenes with visible twinning. Some samples show minor veins of biotite and quartz filled vugs, despite not being associated with ore-forming mineralisation. Rare minor oxides include magnetite. Samples from Vatia lack biotite but contain large amounts of euhedral amphibole, and coarse (<0.5 mm) plagioclase crystals.

2.8.3. Post-subduction shoshonites

Post-subduction shoshonites across Fiji have similar bulk mineralogy, although their mafic mineral compositions do vary. The shoshonite series is divided into absarokites (clinopyroxene-phyric, with less common olivine phenocrysts, variable proportions of plagioclase phenocrysts, and plagioclase and magnetite microphenocrysts); shoshonite (plagioclase phyric, with less clinopyroxene); and banakites (with ubiquitous biotite, and commonly plagioclase phenocrysts) (Rogers and Setterfield, 1994).

The Navilawa Monzonite at Tuvatu is the intrusive equivalent to the Sabeto volcanics, which have been described elsewhere as 'augite-biotite flows' (Gill & Whelan, 1989), dominated by biotite and pyroxene phenocrysts (Fig. 6 a and b), and thus comparable to the more evolved (shoshonitic to banakitic) portion of the shoshonite series. Two types of biotite are present at Tuvatu, comprising ~15% of thin section area. Primary biotites are often altered and overgrown with dark green chlorite. A second set of pristine, tabular biotites are observed, and where samples are collected close to mineralisation crystals can reach >2 cm in length, suggesting these biotites have a secondary, hydrothermal origin. Minor phlogopite is also present. Pyroxene phenocrysts show normal zoning and twinning and make up 10–20% area. Whilst
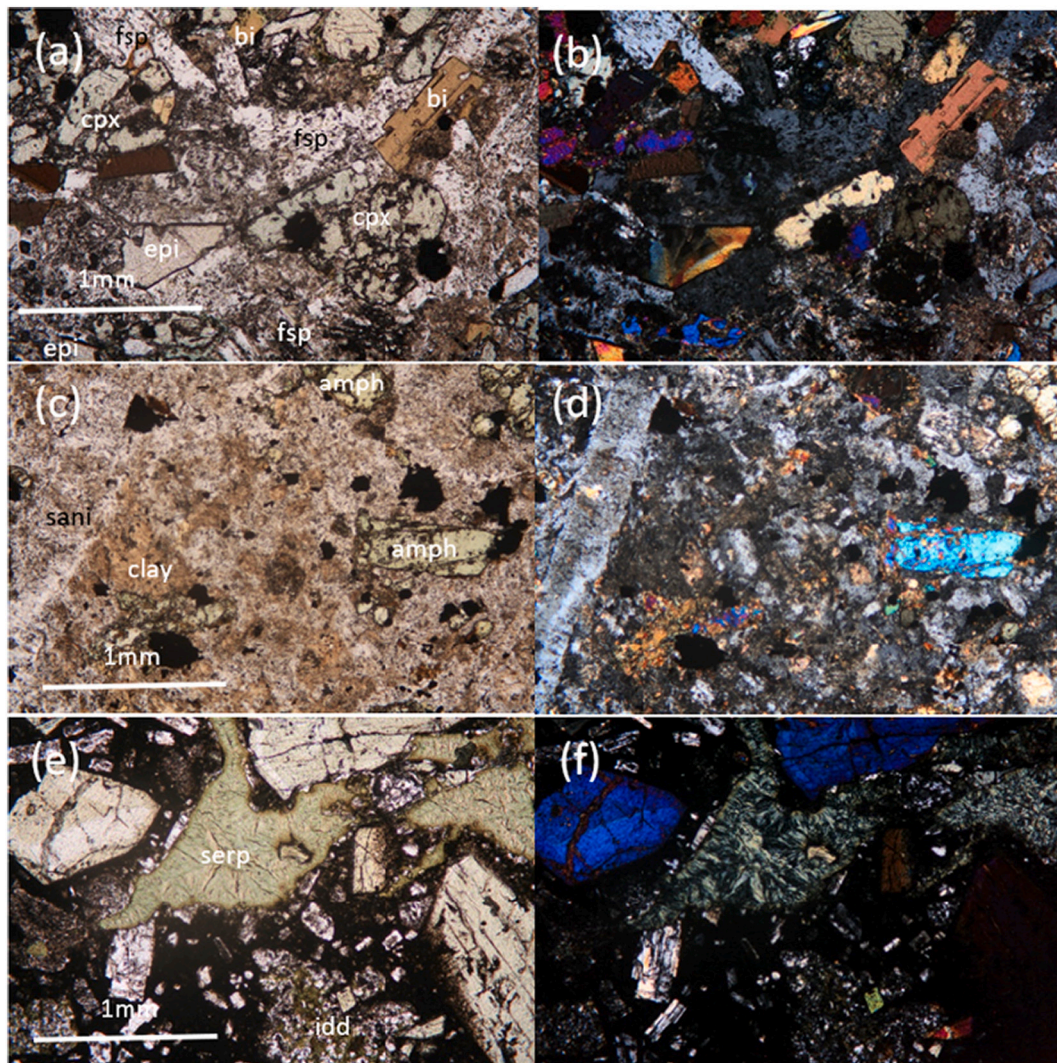
Fig. 6. Thin sections of post-subduction phase rocks using transmitted light: left-hand image plane-polarised and right-hand image cross-polarised light of the same view. FOV always 3 mm across. (a) and (b) show a section from Tuvatu, with biotite (bi) and clinopyroxene (cpx) phenocrysts, coarse angular epidote (*epi*) crystal and feldspar (fsp) dominated groundmass. (c) and (d) are from Sabeto core and show atypical coarse sanidine (sani) crystal at the left, along with clays and minor amphiboles (amph). (e) and (f) show heavily altered core from Raki-Raki, with mafics altered to serpentine, chlorite and iddingsite (idd), serpentine vug fill (serp); fine feldspar crystals can be seen through heavily altered groundmass.

biotites are more abundant, pyroxenes are coarser and dominate volumetrically. Other alteration minerals include unusually coarse, angular epidote crystals; smaller, lime green epidotes; minor quartz and carbonate; abundant magnetite; occasional euhedral apatites; and rare disseminated pyrite. Brown clays are common in the groundmass.

Samples from Tuvatu lack amphibole – a trait in common with samples from the Tavua caldera, but not at other locations, e.g., Sabeto, where small hornblende crystals are seen (Fig. 6 c and d). Members of the Koroimavua group (part of Sabeto area) lack biotite, as do some members of the Ba Group of Vatukoula. Whilst olivine is rare, it is present in samples from Vatukoula (as observed in hand samples) and Raki-Raki (Fig. 6 e and f), although it is now altered to serpentine/iddingsite.

Across all centres, the groundmass is composed of feldspars which, even in the least altered rocks, are altered to white micas including sericite. Feldspars include orthoclase and plagioclase, both of which are often coarse grained (>3 mm), sometimes poikilitic, and occasionally form part of a phaneritic texture. At Tuvatu >50% of thin section area is made up of feldspars, a trait common amongst post-subduction shoshonites. Weak potassic alteration in a few samples is expressed through large secondary biotites, potassium feldspar and replacement of pyroxenes with biotite.

2.8.4. Post-subduction andesitic dykes (Tuvatu)

Post-subduction andesitic dykes at Tuvatu are shown in Fig. 7. They are fine-grained, with a groundmass dominated by laths of plagioclase that have altered centres. Phenocrysts are also small, with even the largest <1 mm in diameter, and are dominated by euhedral clinopyroxenes including diopside. These are far more abundant than in the shoshonites and show exsolution along cleavage planes and inclusions of apatite. Biotite is also present a phenocryst, though in lesser amounts. Minor opaques present include common magnetite and rare pyrite. Although the dykes cross-cut and post-date the Navilawa Monzonite, and are not associated with mineralisation, some light alteration does occur, in the form of minor veinlets of sericite and epidote in some samples.

No samples of post-subduction high-Nb basalts were analysed, although they are described elsewhere as being dominated by olivine and plagioclase with minor amounts (if present) of augite (Gill & Whelan, 1989).

2.9. Geochemistry

2.9.1. Alteration

Although an effort was made to collect the least altered samples available, the petrographic study revealed minor but common alteration as a result of weathering or hydrothermal alteration (for samples spatially associated with mineralisation). To study the impact of alteration, fluid mobile elements have been plotted against loss on ignition (LOI), as an alteration proxy. This allows exploration of any link between alteration and distinctive geochemical trends (Fig. 8).

Firstly, it is important to note that LOI spans a much larger range (up to 10 wt%) than is often expected for magmatic rocks, where values of ~1 are common. However, most values fall below 3, which is reasonable for rocks containing hydrous minerals such as biotite or amphibole. The highest concentrations of the fluid mobile elements are reached at relatively low LOI values of ~2.5, and no robust correlation is shown between LOI and K_2O, Ba, Pb or Rb. It can hence be considered that alteration is not responsible for any significant and systematic trends in fluid mobile elements, and that many geochemical or mineralogical signatures are representative of magmatic processes. However, where LOI is >3, data are treated carefully, with outliers rejected.

To investigate alteration further, two common major element alteration indices have been calculated for all samples and are shown in Fig. 9. These include the Ishikawa alteration index, AI (eq. 1; (Ishikawa et al., 1976)) and chlorite-carbonate-pyrite index, CCPI (eq. 2; (Large, 2001)):

$$AI = 100^* (K_2O + MgO)/(K_2O + MgO + Na_2O + CaO) \qquad (1)$$

$$CCPI = 100^* (FeO_T + MgO)/(FeO_T + MgO + Na2O + CaO) \qquad (2)$$

Values are comparable to those for least altered rocks, whereby AI values between 20 and 65, and CCPI between 20 and 80. CCPI also increases with SiO_2, but when plotted against LOI, there is no correlation, suggesting this is not an artefact of alteration, but rather precursory compositions (Mathieu, 2018).

2.10. Geochemical classifications

Major element data are listed in Table 2. Samples span a range of SiO_2 and MgO contents, 44–73 wt% and 0–12 wt% respectively. Results show distinct differences between magmas of different ages, with one of the best defined being the decoupling in TAS-space between the subalkaline *syn*-subduction samples and alkaline post-subduction samples (Fig. 10). Fijian syn-subduction suites are composed mostly of medium-K andesites and tholeiites, and Fig. 10 inset shows many in the calc-alkaline series. Transitional rocks are also most frequently subalkaline, with a few above the alkaline divide (Irvine and Baragar, 1971).

Post-subduction shoshonites often fall in the 'shoshonite series' or 'high-K alkaline series' fields, although a few at lower silica contents also fall into the calc-alkaline series. Late-stage post-subduction andesitic dykes at Tuvatu appear relatively alkaline, with some samples crossing the thresholds into shoshonitic and potassic. No high-Nb basalts sit in the high-K series or above the potassic line, illustrating a change in composition.

2.10.1. Silica saturation

Silica saturation, based on normative mineralogy, has been calcu-
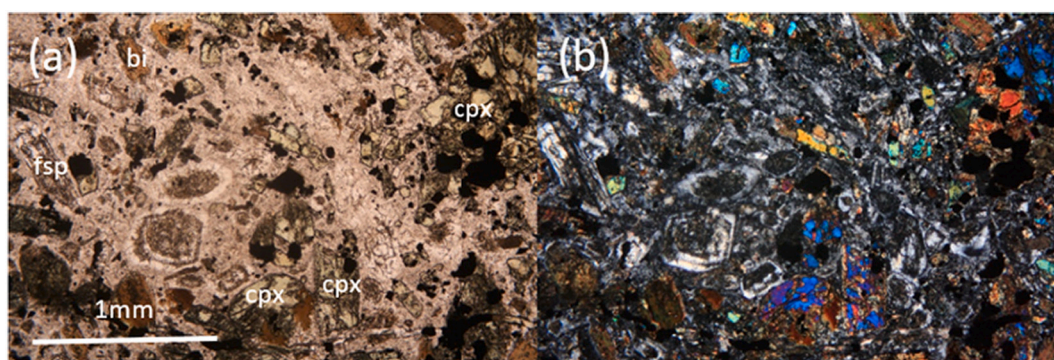
Fig. 7. Thin sections of late-stage andesite dykes are Tuvatu, using transmitted light, (a) showing plane-polarised light and (b) cross-polarised light of the same view. FOV always 3 mm across.
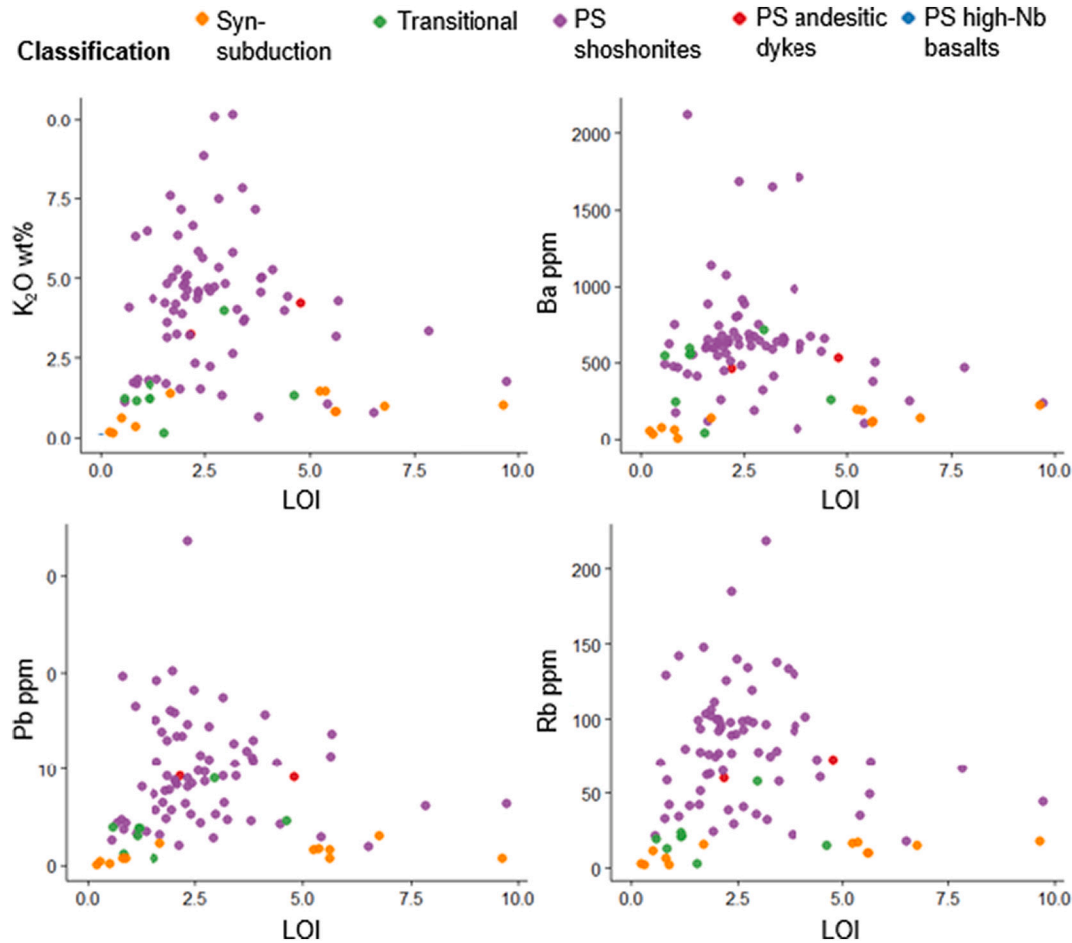
Fig. 8. Graphs showing loss on ignition (LOI) vs the fluid mobile elements K, Ba, Pb and Rb, to explore any correlation or relationship between the two.

lated using CIPW norms, followed by eq. (3) to calculate silica saturation index (SSI):

$$SSI = (\text{hypersthene} + 4Qtz - \text{Neph})/(\text{Hypersthene} + \text{Diops.} + 4Qtz + \text{Neph}) \tag{3}$$

Syn-subduction and transitional calc-alkaline samples are silica-saturated (SSI = 0.5 to 1). Post-subduction shoshonites, post-subduction andesitic dykes and post-subduction high-Nb basalts, generally fall below SSI 0.5, with many samples sitting below the zero line. The Navilawa Monzonite from Tuvatu is the least silica saturated, and the median value for samples from Tuvatu is around −0.2. Overall, the evolution of magmatism is from *syn*-subduction silica-saturated tholeiites, through calc-alkaline intermediate suites; transitional phase alkaline and silica under-saturated potassic to ultra-potassic shoshonites; and under-saturated alkaline to calc-alkaline basalts and minor dykes in the remnant arc phase.

2.10.2. Major element geochemistry

Fig. 11 shows variation diagrams of major elements vs SiO_2, where all groups follow many similar trends: Na_2O contents increase with increasing SiO_2 and fraction, and Fe_2O_3, MgO and CaO contents decrease with increasing SiO_2.

No group can be distinguished in Na_2O space, as all show a slightly positive trend – though this is less distinct with subduction samples than others. All groups differ from post-subduction shoshonites in K_2O space, with subduction samples remaining relatively constant; K_2O rarely exceeds 2 wt%.

In addition, *syn*-subduction samples show no systematic variations in Al_2O_3 or MnO with evolution. They have relatively high TiO_2, MgO and

CaO when compared to all other groups except the high-Nb basalts; this is especially pronounced when compared to post-subduction shoshonites, although at low SiO_2 their contents show some overlap. Whilst TiO_2 is relatively elevated, it maintains a flat trend at ~1 wt. The same is seen in P_2O_5, which maintains a plateau at around 0.2 wt%, generally lower than other groups. No robust trend for Fe_2O_3 can be discerned.

The transitional samples mostly overlap with the syn-subduction samples although there is some similarity between with post-subduction shoshonites, showing their transitional nature. Post-subduction shoshonites have consistently lower TiO_2, MgO and CaO, and higher P_2O_5 than any other group. As illustrated in previous diagrams, the K-enrichment in post-subduction shoshonites seems to be present even at low SiO_2. Unlike subduction samples, post-subduction shoshonites show a coherent decrease in Fe_2O_3 and increase in Al_2O_3 with increasing SiO_2. Strong trends including increasing Al_2O_3 and decreasing MgO are present at low SiO_2. MnO shows no obvious trend.

Post-subduction high-Nb basalts often form a distinct domain, with patterns offset from those of other classification groups. The clearest example of this is for TiO_2, where contents reach over double those of other samples. This is also reasonably pronounced in Na_2O, CaO and MgO space. Late-stage dykes, like post-subduction samples, are indistinguishable from other trends.

2.10.3. Trace element geochemistry

Trace element data (Table 3) are displayed as bivariate plots of trace elements against SiO_2 contents (Fig. 12) and as multi-element plots (Fig. 13, Fig. 14). The transition elements Cr, Ni, and V display similar contents and trends with evolution across all categories.

Syn-subduction rocks show many characteristics typical for arc rocks
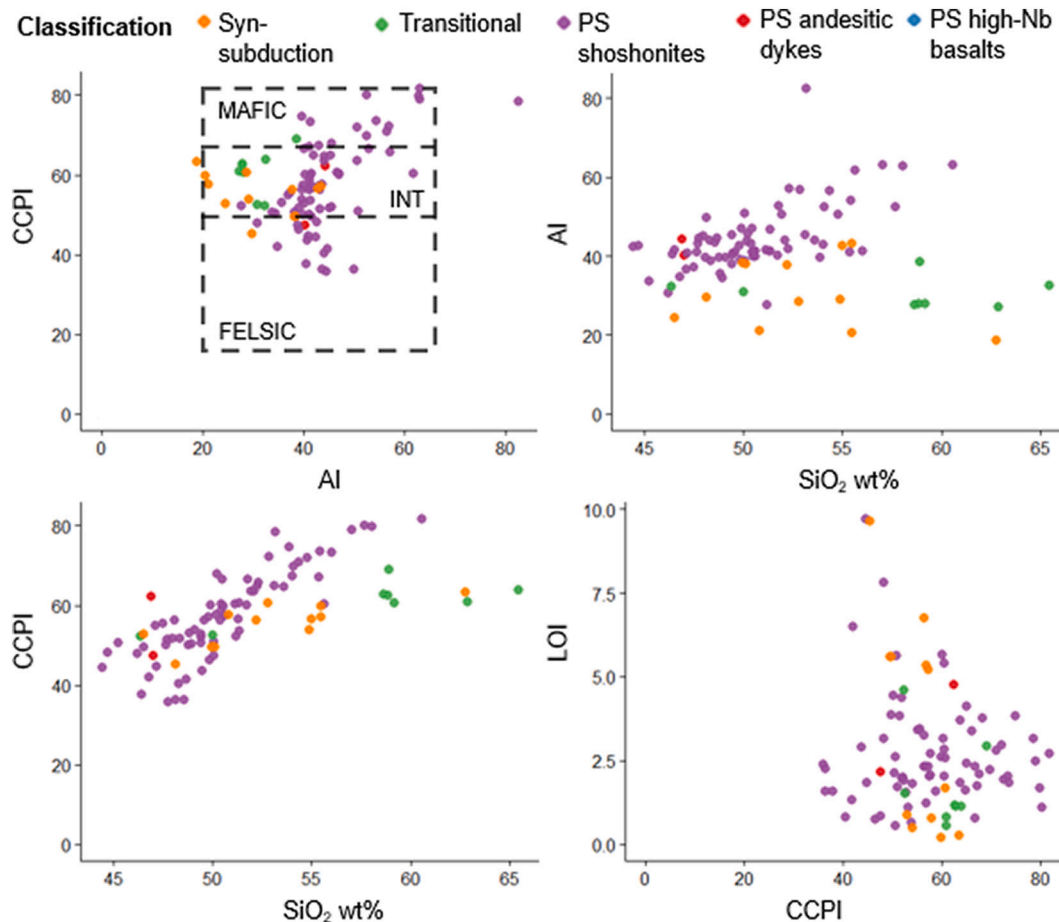
Fig. 9. Plots showing major element alteration indices AI (Ishikawa et al., 1976) and CCPI (Large et al., 2001) plotted against each other in an alteration box plot, against SiO_2 (as a function of evolution) and CCPI against LOI.

and processes, although trends for large ion lithophile elements (LILE) are peculiar, with little to no correlation between Pb, Rb and Sr (and K) against SiO_2. Instead, concentrations remain low across all silica contents, and lower than anticipated when compared to other arcs normalised to MORB (Fig. 13). Other high field-strength elements (HFSE) such as Th and U also follow this pattern, remaining at low concentrations. Incompatible elements have overall low concentrations and no systematic correlation with fractionation.

In *syn*-subduction tholeiites, high field-strength elements (HFSE) are generally low concentration, with a weakly positive relationship with SiO_2. MORB-normalised multi-element patterns (Fig. 13) are relatively flat, with slight enrichment of LILE and no shift in pattern with changing SiO_2. The same is true for patterns in Fig. 14 as REE contents remain stable with evolution and primary data showing no systematic changes.

Similar to major element patterns, transitional samples show little distinction although their concentrations often fall between those for *syn*-subduction and post-subduction shoshonites. This is especially clear in median values in Fig. 13 and Fig. 14, and is the case for LILE, HFSE and the REEs (though data show much variation). That said, many trends in Fig. 12 show more similarity to subduction trends, with scatter, relatively flatter trends for Ba, Pb, Rb and Sr, and comparable concentrations of Sc, U and Zr.

Post-subduction shoshonites show an accentuation of 'normal' arc enrichment patterns, with steep positive trends between SiO_2 and Ba, Ce, La, Nd, Pb, Rb, Sr, Th and U, and high concentrations of these elements even at low SiO_2. Barium, K, Pb, and Rb reach remarkably high values when compared to global arc rocks (Schmidt and Jagoutz, 2017), although Th and U remain comparatively low. Values for most HFSE compared to MORB are ~1, and Fig. 13 highlights a pronounced Nb—Ta

trough, typical for arc-rocks but more pronounced in shoshonites than syn-subduction samples. Low concentrations of other HFSE encompasses Ti, Y, and Zr, although the latter appears to marginally increase with evolution. The LREEs also remain relatively enriched, especially when compared to HREEs.

High-Nb basalts show the most distinction from other groups, with elevated concentrations of Nb rather than a trough; low-intermediate levels of Rb and Sr; and consistently higher values in HFSE and REE, especially La, Ce, Nd, Zr and Ti. Therefore, they have a much flatter pattern in Fig. 13, and samples sit in a distinct domain when plotted against SiO_2 for Zr in Fig. 12. Due to this data being obtained from literature, data is missing from Fig. 14 as many REE elements are not published.

3. Discussion

As the geodynamic setting of the Fiji Platform has changed from intra-oceanic arc, to collision/compression through to extension/rotation, to compression/rotation and cessation of volcanism on Viti Levu, so have the geochemical characteristics of the magmatism. Early arc activity is tholeiitic to calc-alkaline, followed by the post-subduction shoshonitic calderas of Viti Levu, and later by uncommon, high-Nb dykes with an affinity to the back-arc basalts of the North Fiji Basin. The shoshonites represent an exotic style of arc magmatism, typically subordinate to the voluminous tholeiitic and calc-alkaline compositions. The Fijian shoshonitic centres show further unusual characteristics in that they are associated with Au-(Te) mineralisation – a phenomenon observed in other shoshonite-series igneous complexes (Jensen and Barton, 2000; Sillitoe, 2002) including: the Goonumbla porphyry Cu

Table 2

Sample description and bulk rock major element chemistry of volcanic and intrusive samples from Viti Levu. All values in wt%.

Sample	Location	Unit	Rock Name	Classification	SiO_2	TiO_2	Al_2O_3	Fe_2O_3	MnO	MgO	CaO	Na_2O	K_2O	P_2O_5	LOI	Total
TU-19-248	Tuvatu	Andesitic Dykes	Andesite'	PS andesitic dykes	46.87	0.81	17.26	11.81	0.18	2.63	6.84	1.79	4.21	0.38	4.79	98.60
TU-19-249	Tuvatu	Andesitic Dykes	Andesite'	PS andesitic dykes	46.99	0.72	15.61	11.70	0.24	5.21	10.62	1.95	3.24	0.34	2.17	99.47
NJ-17-02.1	Natovi Jetty	Ba Group	Basalt	Post-subduction shoshonites	48.66	0.92	14.31	10.60	0.20	8.54	9.79	3.04	1.83	0.41	1.35	99.65
NJ-17-02.2	Natovi Jetty	Ba Group	Basalt	Post-subduction shoshonites	48.28	0.97	15.18	10.25	0.16	8.85	11.52	1.85	1.70	0.46	0.83	100.07
NJ-17-03.2	Natovi Jetty	Ba Group	Basalt	Post-subduction shoshonites	48.90	0.93	18.56	11.02	0.18	5.79	10.80	2.40	1.14	0.22	0.56	100.49
VM-17-01.1	Vatukoula	Ba Group	Absarokite	Post-subduction shoshonites	48.54	0.56	12.82	10.11	0.16	8.35	12.14	1.66	2.35	0.38	2.28	99.38
VM-17-02.1	Vatukoula	Ba Group	Basalt	Post-subduction shoshonites	47.73	0.58	12.34	11.09	0.15	8.88	11.31	1.66	1.55	0.35	2.40	100.16
VM-17-04.1	Vatukoula	Ba Group	Shoshonite	Post-subduction shoshonites	53.88	0.53	19.62	5.83	0.17	1.27	4.74	4.15	4.57	0.44	3.84	99.04
VM-17-05	Vatukoula	Ba Group	Shoshonite	Post-subduction shoshonites	57.69	0.46	19.64	4.65	0.16	1.26	3.13	3.90	6.49	0.31	1.11	98.81
VM-17-06.1	Vatukoula	Ba Group	Andesite	Post-subduction shoshonites	51.79	0.63	18.58	7.83	0.20	3.07	5.43	2.50	5.83	0.59	2.35	98.80
VM-17-07	Vatukoula	Ba Group	Basalt	Post-subduction shoshonites	48.14	0.58	13.82	10.56	0.18	11.31	10.82	2.22	1.69	0.30	1.59	101.23
VM-17-09.1	Vatukoula	Ba Group	Andesite	Post-subduction shoshonites	56.00	0.49	19.36	5.35	0.24	1.53	4.88	4.18	4.85	0.35	2.04	99.27
FAD-50-01	Fadis	Fadis	Shoshonite	Post-subduction shoshonites	50.23	1.69	17.24	13.55	0.27	5.32	2.07	5.05	0.65	0.24	3.79	100.12
FAD-50-02	Fadis	Fadis	Shoshonite	Post-subduction shoshonites	55.62	0.90	15.84	8.42	0.34	7.25	2.32	2.86	1.08	0.26	5.42	100.36
RR-17-02.1	Rakiraki	Raki-Raki	Shoshonite	Post-subduction shoshonites	50.03	0.83	16.51	9.69	0.14	6.40	10.20	2.78	1.83	0.30	0.87	99.58
RR-17-03.1	Rakiraki	Raki-Raki	Shoshonite	Post-subduction shoshonites	49.85	0.81	16.20	9.88	0.15	6.67	10.37	2.74	1.75	0.29	0.77	99.49
TBH-004-18	Rakiraki	Raki-Raki	Shoshonite	Post-subduction shoshonites	44.40	0.72	14.93	9.17	0.15	6.95	9.96	1.89	1.79	0.22	9.72	100.35
TDH-004-06	Rakiraki	Raki-Raki	Shoshonite	Post-subduction shoshonites	46.78	0.74	15.23	9.01	0.19	6.81	12.40	1.90	0.81	0.11	6.51	100.53
TDH-004-16	Rakiraki	Raki-Raki	Shoshonite	Post-subduction shoshonites	49.48	0.76	15.55	9.94	0.17	7.20	11.08	1.37	1.35	0.23	2.92	100.09
TDH-004-17	Rakiraki	Raki-Raki	Shoshonite	Post-subduction shoshonites	49.39	0.72	16.64	10.10	0.16	5.48	9.28	3.26	2.26	0.34	2.62	100.34
FJ-19-01	Sabeto	Sabeto Group	Shoshonite	Post-subduction shoshonites	49.40	0.73	17.49	9.40	0.19	4.52	9.75	3.30	4.24	0.56	1.55	101.16
FJ-19-02	Sabeto	Sabeto Group	Shoshonite	Post-subduction shoshonites	47.62	0.70	16.39	8.58	0.17	4.62	10.28	2.67	4.43	0.25	4.46	100.21
FJ-19-03	Sabeto	Sabeto Group	Shoshonite	Post-subduction shoshonites	51.27	0.57	18.57	8.20	0.18	3.90	9.00	2.66	4.37	0.44	1.25	100.43
SBDD-0001-01	Sabeto	Sabeto Group	Shoshonite	Post-subduction shoshonites	54.76	0.52	18.65	5.86	0.11	2.86	3.67	3.81	4.83	0.28	2.99	99.36
SBDD-0001-04	Sabeto	Sabeto Group	Shoshonite	Post-subduction shoshonites	54.35	0.44	18.53	5.36	0.20	1.88	5.06	2.15	7.48	0.21	2.83	98.79
SBDD-0002-16	Sabeto	Sabeto Group	Shoshonite	Post-subduction shoshonites	47.93	0.73	16.45	8.43	0.27	5.25	8.72	2.56	4.01	0.34	4.39	99.52
SBDD-0003-01	Sabeto	Sabeto Group	Shoshonite	Post-subduction shoshonites	55.35	0.46	17.48	6.52	0.11	2.40	5.34	3.84	4.00	0.26	1.76	99.32
SBDD-0003-08	Sabeto	Sabeto Group	Shoshonite	Post-subduction shoshonites	53.12	0.49	18.23	6.89	0.25	2.40	6.56	3.15	5.66	0.33	2.44	99.56
SBDD-0003-13	Sabeto	Sabeto Group	Shoshonite	Post-subduction shoshonites	55.41	0.56	19.00	5.44	0.14	2.51	3.69	3.76	6.34	0.31	1.87	99.41
SBDD-0003-29	Sabeto	Sabeto Group	Shoshonite	Post-subduction shoshonites	52.25	0.47	18.09	6.08	0.21	2.27	6.65	3.77	5.28	0.28	4.12	99.51
SBDD-0003–41	Sabeto	Sabeto Group	Shoshonite	Post-subduction shoshonites	51.72	0.49	17.00	6.84	0.25	2.91	7.42	3.28	4.31	0.33	5.67	100.25
SR-17-01.1	Sabeto River	Sabeto Group	Shoshonite	Post-subduction shoshonites	44.66	1.16	16.63	10.67	0.19	7.01	9.32	3.66	2.63	0.29	3.18	99.57
SR-17-01.2	Sabeto River	Sabeto Group	Andesite	Post-subduction shoshonites	54.04	0.52	18.32	6.27	0.16	2.32	5.69	4.12	5.10	0.28	2.10	99.19
SR-17-02.1	Sabeto River	Sabeto Group	Shoshonite	Post-subduction shoshonites	48.83	0.89	18.41	10.19	0.18	5.08	9.65	2.86	1.82	0.29	1.12	99.35
SR-17-02.2	Sabeto River	Sabeto Group	Shoshonite	Post-subduction shoshonites	46.40	0.77	12.11	11.15	0.20	6.77	11.54	3.72	3.62	1.00	1.60	99.11
TU-19-009	Tuvatu	Sabeto Group	Monzonite	Post-subduction shoshonites	51.12	0.62	18.52	7.01	0.17	3.15	7.88	3.64	5.04	0.43	2.05	99.69
TU-19-010	Tuvatu	Sabeto Group	Monzonite	Post-subduction shoshonites	49.76	0.68	18.03	7.77	0.20	3.97	8.35	3.11	4.60	0.48	2.35	99.45
TU-19-035	Tuvatu	Sabeto Group	Monzonite	Post-subduction shoshonites	50.42	0.66	18.16	7.56	0.20	3.38	8.25	3.50	4.84	0.47	1.61	99.42
TU-19-036	Tuvatu	Sabeto Group	Monzonite	Post-subduction shoshonites	50.53	0.65	18.16	7.48	0.19	3.44	7.68	3.68	4.59	0.46	2.64	99.62
TU-19-040	Tuvatu	Sabeto Group	Monzonite	Post-subduction shoshonites	50.36	0.68	18.02	7.80	0.19	3.99	8.67	2.47	4.52	0.48	2.34	99.55
TU-19-048	Tuvatu	Sabeto Group	Monzonite	Post-subduction shoshonites	50.44	0.68	18.09	7.71	0.24	3.57	7.22	2.78	5.32	0.48	2.84	99.46
TU-19-049	Tuvatu	Sabeto Group	Monzonite	Post-subduction shoshonites	50.15	0.67	18.08	7.82	0.25	3.74	8.38	2.54	4.74	0.47	2.73	99.65
TU-19-050	Tuvatu	Sabeto Group	Monzonite	Post-subduction shoshonites	50.61	0.67	18.16	7.72	0.25	3.49	8.73	2.85	4.64	0.47	2.09	99.72
TU-19-051	Tuvatu	Sabeto Group	Monzonite	Post-subduction shoshonites	50.60	0.67	18.09	7.59	0.24	3.41	8.82	2.99	4.45	0.47	2.05	99.44
TU-19-055	Tuvatu	Sabeto Group	Monzonite	Post-subduction shoshonites	54.08	0.49	19.17	5.78	0.19	2.44	5.12	3.11	6.66	0.36	2.22	99.66
TU-19-056	Tuvatu	Sabeto Group	Monzonite	Post-subduction shoshonites	51.92	0.51	18.17	5.60	0.23	2.37	7.10	2.22	7.15	0.36	3.70	99.36
TU-19-086	Tuvatu	Sabeto Group	Monzonite	Post-subduction shoshonites	57.03	0.40	19.43	3.31	0.10	1.51	3.16	2.89	8.84	0.06	2.48	99.59
TU-19-089	Tuvatu	Sabeto Group	Monzonite	Post-subduction shoshonites	60.57	0.19	17.90	0.89	0.13	0.26	3.37	2.69	10.12	0.14	2.73	99.58
TU-19-101	Tuvatu	Sabeto Group	Monzonite	Post-subduction shoshonites	52.28	0.50	17.75	5.88	0.22	2.67	5.70	2.15	7.83	1.14	3.41	99.65
TU-19-112	Tuvatu	Sabeto Group	Monzonite	Post-subduction shoshonites	46.17	0.60	16.20	7.31	0.15	3.08	12.82	1.61	3.35	0.42	7.82	99.63
TU-19-113	Tuvatu	Sabeto Group	Monzonite	Post-subduction shoshonites	48.34	0.75	17.06	8.95	0.20	4.26	10.19	2.53	3.88	0.51	1.98	99.43
TU-19-120	Tuvatu	Sabeto Group	Monzonite	Post-subduction shoshonites	47.09	0.70	18.69	8.08	0.15	3.73	10.09	2.58	3.67	0.50	3.42	98.76
TU-19-128	Tuvatu	Sabeto Group	Monzonite	Post-subduction shoshonites	49.39	0.72	15.97	9.02	0.15	4.61	8.79	2.44	4.77	1.29	2.00	99.25
TU-19-159	Tuvatu	Sabeto Group	Monzonite	Post-subduction shoshonites	58.04	0.53	19.29	2.87	0.06	2.81	1.62	4.53	7.58	0.18	1.69	99.49

Table 2 (*continued*)

Sample	Location	Unit	Rock Name	Classification	SiO$_2$	TiO$_2$	Al$_2$O$_3$	Fe$_2$O$_3$	MnO	MgO	CaO	Na$_2$O	K$_2$O	P$_2$O$_5$	LOI	Total
TU-19-160	Tuvatu	Sabeto Group	Monzonite	Post-subduction shoshonites	65.81	0.03	17.75	0.27	0.00	0.04	0.38	1.76	12.61	0.24	0.38	99.28
Sample	*Location*	*Unit*	*Rock Name*	*Classification*	*SiO2*	*TiO2*	*Al2O3*	*Fe2O3*	*MnO*	*MgO*	*CaO*	*Na2O*	*K2O*	*P2O5*	*LOI*	*Total*
TU-19-178	Tuvatu	Sabeto Group	Monzonite	Post-subduction shoshonites	47.48	0.74	17.52	8.44	0.19	3.74	9.07	3.53	3.73	0.50	3.45	98.46
TU-19-210	Tuvatu	Sabeto Group	Monzonite	Post-subduction shoshonites	53.59	0.96	15.71	12.50	0.17	3.47	4.33	4.06	3.16	0.07	1.62	99.85
TU-19-213	Tuvatu	Sabeto Group	Monzonite	Post-subduction shoshonites	48.07	0.75	17.86	9.09	0.21	3.71	8.88	2.84	4.02	0.54	3.26	99.48
TU-19-238	Tuvatu	Sabeto Group	Monzonite	Post-subduction shoshonites	49.08	0.74	17.47	8.73	0.20	4.09	9.46	3.17	4.21	0.51	1.82	99.64
TU-19-250	Tuvatu	Sabeto Group	Monzonite	Post-subduction shoshonites	45.23	0.68	15.82	11.20	0.30	3.29	10.82	1.96	3.20	0.52	5.63	99.31
TU-19-251	Tuvatu	Sabeto Group	Monzonite	Post-subduction shoshonites	51.15	0.81	17.07	8.58	0.15	3.88	10.31	3.81	1.55	0.26	1.93	99.57
TU-19-252	Tuvatu	Sabeto Group	Monzonite	Post-subduction shoshonites	47.17	0.74	15.45	11.13	0.22	5.96	11.53	1.77	3.24	0.42	1.84	99.53
TU-19-253	Tuvatu	Sabeto Group	Monzonite	Post-subduction shoshonites	49.90	0.64	18.21	7.32	0.20	3.42	7.59	2.79	5.81	0.43	3.17	99.62
TU-19-254	Tuvatu	Sabeto Group	Monzonite	Post-subduction shoshonites	47.66	0.66	16.14	9.98	0.29	3.92	10.05	1.67	5.01	0.43	3.83	99.65
TU-19-255	Tuvatu	Sabeto Group	Monzonite	Post-subduction shoshonites	46.49	0.68	15.76	9.88	0.33	3.79	10.96	1.43	5.02	0.43	3.86	98.67
TUDDH-398a	Tuvatu	Sabeto Group	Monzonite	Post-subduction shoshonites	51.34	0.67	16.85	9.24	0.15	4.33	8.89	3.03	4.08	0.50	0.67	99.80
TUDDH-398b	Tuvatu	Sabeto Group	Monzonite	Post-subduction shoshonites	48.75	0.74	16.92	9.49	0.19	5.21	10.08	2.64	3.21	0.38	2.14	99.83
TUDDH-408a	Tuvatu	Sabeto Group	Monzonite	Post-subduction shoshonites	49.58	0.72	18.07	8.24	0.19	3.97	8.73	3.16	4.35	0.51	2.33	100.03
TUDDH-415	Tuvatu	Sabeto Group	Monzonite	Post-subduction shoshonites	51.36	0.67	18.66	7.55	0.18	3.87	7.15	2.62	4.68	0.48	2.59	99.88
TUDDH-427	Tuvatu	Sabeto Group	Monzonite	Post-subduction shoshonites	52.85	0.65	18.09	6.61	0.12	1.90	4.35	2.51	7.14	0.41	1.94	98.77
TUDDH-437	Tuvatu	Sabeto Group	Monzonite	Post-subduction shoshonites	50.07	0.65	15.52	9.92	0.26	5.55	8.15	2.08	5.03	0.51	1.74	99.58
TUDDH-456	Tuvatu	Sabeto Group	Monzonite	Post-subduction shoshonites	52.09	0.61	18.82	6.86	0.18	3.00	6.77	3.71	5.26	0.43	1.87	99.67
TUDDH-463b	Tuvatu	Sabeto Group	Monzonite	Post-subduction shoshonites	53.16	0.69	17.86	7.28	0.06	3.20	1.23	1.60	10.18	0.63	3.16	99.26
TUDDH-469	Tuvatu	Sabeto Group	Monzonite	Post-subduction shoshonites	50.46	0.44	17.99	5.03	0.15	1.95	6.23	6.16	6.32	0.34	0.80	98.65
FJ-19-04a	Vatia	Suva Group	Andesite	Post-subduction shoshonites	58.62	0.58	18.40	6.36	0.11	2.82	7.03	3.49	1.25	0.17	1.16	99.99
FJ-19-04b	Vatia	Suva Group	Andesite	Post-subduction shoshonites	58.86	0.59	18.34	6.37	0.12	2.87	7.03	3.50	1.22	0.17	1.19	100.25
FJ-19-05	Vatia	Suva Group	Andesite	Post-subduction shoshonites	59.15	0.56	18.06	5.95	0.13	3.11	7.48	3.66	1.23	0.17	0.57	100.09
LL-17-01.1	Lomolomo	Suva Group	Andesite	Transitional	58.91	0.49	20.21	6.05	0.16	2.41	5.86	4.36	4.00	0.33	2.95	108.12
MQ-17-01.1	Mau Quarry	Suva Group	Andesite	Transitional	65.42	0.73	18.98	6.89	0.11	3.32	6.41	3.92	1.66	0.20	1.16	108.86
NJ-17-01.1	Natovi Jetty	Suva Group	Basalt	Transitional	46.35	0.95	17.41	9.59	0.11	5.07	9.34	4.09	1.33	0.38	4.62	99.26
NR-17-01.3	Navua River	Suva Group	Andesite	Transitional	49.98	1.09	16.46	11.77	0.30	5.43	8.26	4.24	0.16	0.12	1.54	99.37
NR-17-01.4	Navua River	Suva Group	Andesite	Transitional	62.86	0.64	15.68	6.03	0.10	2.54	6.60	3.31	1.17	0.12	0.83	99.88
BB-17-01.2	Balenbelo	Wainimala Group	Andesite	Syn-subduction	55.46	1.06	17.78	10.68	0.24	2.87	8.04	3.71	0.18	0.10	0.21	100.34
BB-17-01-1	Balenbelo	Wainimala Group	Andesite	Syn-subduction	62.74	0.76	16.13	7.64	0.19	2.16	6.36	3.61	0.15	0.12	0.29	100.16
FJ-19-06ai	Tuvatu-area	Wainimala Group	Breccia	Syn-subduction	49.95	0.93	15.64	9.41	0.17	6.05	8.48	2.57	0.82	0.12	5.60	99.97
FJ-19-06aii	Tuvatu-area	Wainimala Group	Breccia	Syn-subduction	50.12	0.92	15.73	9.34	0.17	6.02	8.48	2.59	0.83	0.11	5.61	100.17
FJ-19-06bi	Tuvatu-area	Wainimala Group	Breccia	Syn-subduction	55.45	0.87	15.47	7.65	0.13	5.12	5.35	3.24	1.46	0.14	5.23	100.26
FJ-19-06bii	Tuvatu-area	Wainimala Group	Breccia	Syn-subduction	54.96	0.86	15.37	7.65	0.13	5.09	5.55	3.19	1.46	0.13	5.36	99.95
FJ–19-06c	Tuvatu-area	Wainimala Group	Breccia	Syn-subduction	52.18	0.76	16.61	8.31	0.11	4.54	7.11	2.01	0.98	0.15	6.76	99.81
FJ-19-07	Tuvatu-area	Wainimala Group	Breccia	Syn-subduction	48.14	1.18	13.51	9.70	0.16	4.18	10.64	1.72	1.03	0.14	9.64	100.07
KV-17-02.1	Koroviolou village	Wainimala Group	Gabbro	Syn-subduction	50.82	0.71	20.77	9.75	0.16	3.10	10.69	2.15	0.36	0.05	0.81	99.42
NR-17-01.1	Navua River	Wainimala Group	Andesite	Syn-subduction	54.90	0.91	16.33	10.62	0.17	4.09	8.64	2.84	0.62	0.15	0.49	99.77
WR-17-01.1	Wanivesi River	Wainimala Group	Andesite	Syn-subduction	52.81	0.81	19.51	7.61	0.12	3.35	8.14	3.72	1.41	0.15	1.68	99.29
WYR-17-01.1	Waydoi River	Wainimala Group	Basalt	Syn-subduction	46.49	0.11	25.14	6.45	0.10	5.17	15.14	0.96	0.03	0.01	0.88	100.58
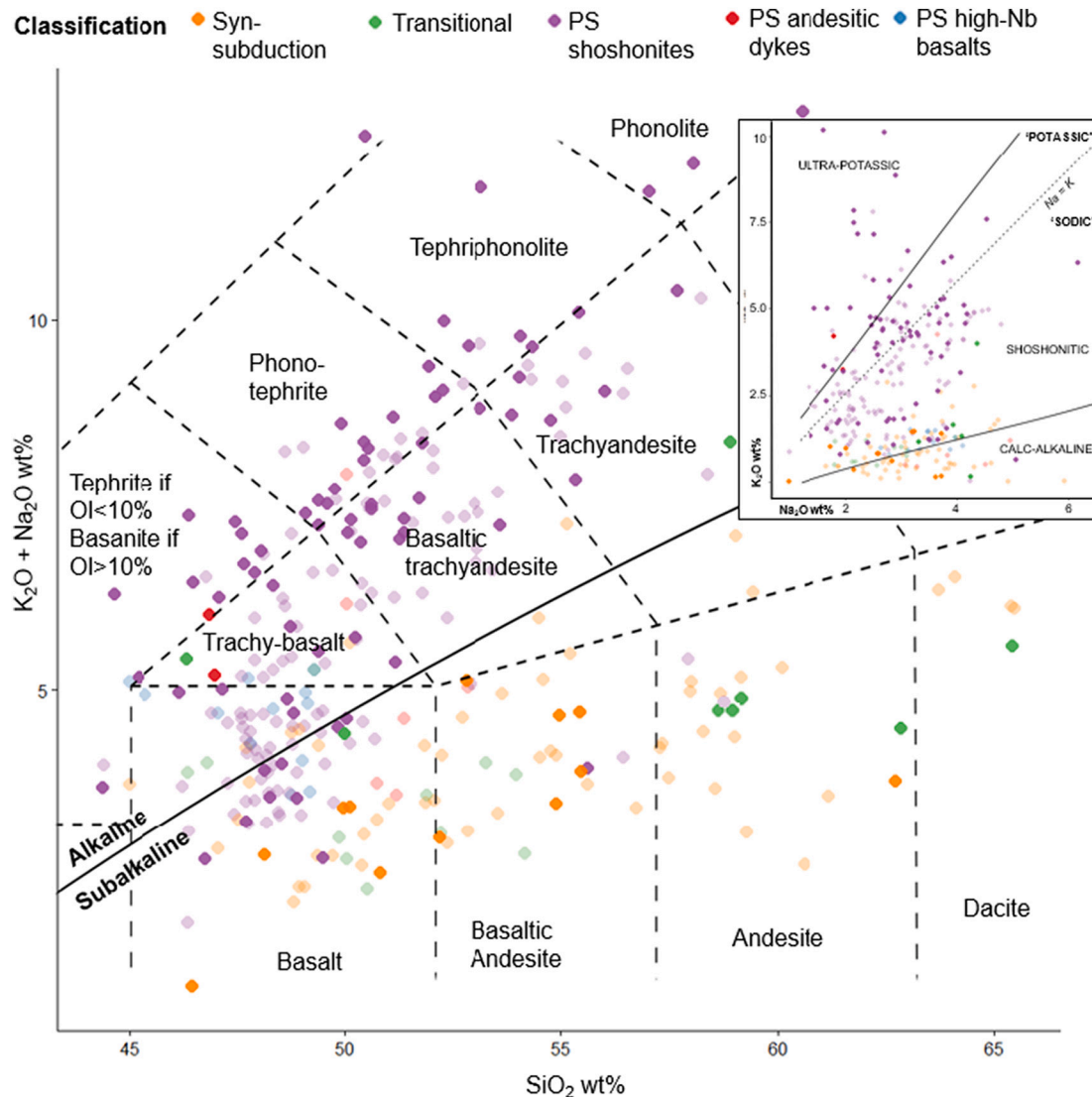
Fig. 10. TAS plot, using classification scheme from Le Bas et al. (1986) and alkaline/subalkaline fields of Irvine and Baragar (1971). The key above the graph shows the classification of sample groups. Points are paler/less opaque in colour where the data has been obtained from literature sources. Post-subduction shoshonites (purple) show alkali enrichment relative to the subduction samples (orange) at intermediate (>50 wt%) SiO₂. Inset: Na₂O against K₂O in wt%, with Na: K molar 1:1 ratio showing the distinction between 'sodic' and 'potassic' rocks as a dashed line, and solid lines showing the rock classifications of Middlemost (1975). (For interpretation of the references to colour in this figure legend, the reader is referred to the web version of this article.)

district, NSW, Australia (Müller et al., 1994); Cripple Creek, Colorado (Kelley and Ludington, 2002); the Didipio Cu—Au deposit, the Philippines (Wolfe and Cooke, 2011); Kalgoorlie's giant Golden Mile (Taylor et al., 1994); and Porgera, Papua New Guinea (Ronacher et al., 2004) – but a departure from the more common associations of Au mineralisation with calc-alkaline hosts in arcs (du Bray, 2017). Here, we discuss the petrogenetic mechanisms and different melt sources through the evolution of Fiji and Viti Levu, and examine the role that post-subduction magmatism has on potential Au—Te fertility.

3.1. Syn-subduction petrogenesis

3.1.1. Fractionation

The diverse lithologies of *syn*-subduction phase magmatism include tholeiitic and calc-alkaline andesite and basalts of the Wainimala Group and Nadele Breccia. Samples are typically crystal-rich, and their chemistry is unlikely to represent a liquid line of descent. Major and trace element bivariate plots (Fig. 11, Fig. 12) confirm this, with considerable scatter of data. Nevertheless, some trends are apparent and indicate that

fractionation is an important process governing the geochemistry of these rocks.

A 'typical' arc magma fractionation assemblage produces patterns that include decreasing Fe_2O_3, MgO, CaO, Cr and Ni, and increasing Al_2O_3. Syn-subduction suites are not entirely consistent with these trends. Biotite, augite, titanite and perhaps hornblende may instead drive trends, especially those of Al_2O_3, Fe_2O_3, MgO, CaO and Na_2O. This aligns reasonably well with observed phenocryst phases, which are dominated by clinopyroxene, plagioclase, and minor biotite and hornblende, but lacking in olivine (Fig. 5). To quantify fractionation assemblages in the absence of observed cumulates, differentiation was modelled using least-squares regression modelling of major element data. Whilst the modelling did resolve, residual errors were relatively high; tables illustrating the models can be found in Appendix 3. Overall, the models further support polymineralic fractionation assemblages containing augite, biotite, and oxides. The modelled fractionating phases also contain plagioclase. All these minerals are observed in studied samples. Trace element vector modelling of fractional crystallisation throughout this time are consistent with pyroxene, plagioclase, and
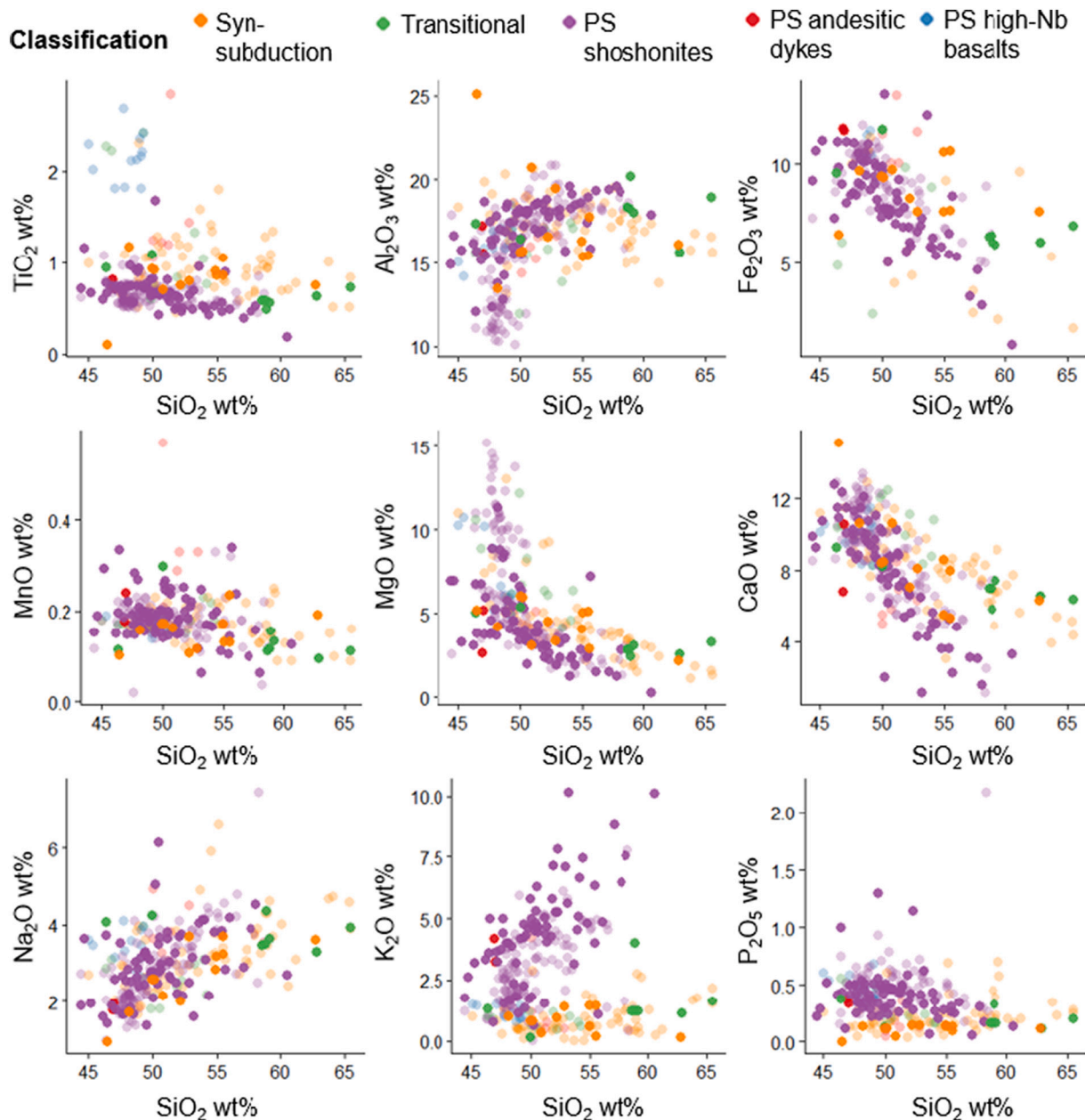
Fig. 11. Bivariate plots showing major element oxides against SiO_2 wt%. Darker/ more opaque dots represent primary data whilst paler dots show literature data – used in this context to better show patterns. Primary data collected using XRF. Any potential error within the values is smaller than or equal to the size of the dot. Most categories show similar patterns overall, with the major distinguishing plot being K_2O.

perhaps minor olivine crystallisation.

Even though it is included in the model, predicted fractionation assemblages commonly lack olivine. This is because, despite modelling using the least evolved sample, it is not likely to be a primitive composition. Models also always lack hornblende, consistent with its rarity as a phenocryst phase (Fig. 5 and Fig. 6). Whilst limited hornblende phenocrysts might permit its presence as a cryptic phase in fractionated assemblages (Davidson et al., 2007; Smith, 2014), trace element patterns and ratios suggest there is only a limited role for amphibole during differentiation. It has been suggested that Sr/Y should be >30 where amphibole fractionation occurs (Moyen, 2009), but *syn*-subduction values remain very low (<10; Fig. 15). Middle REE have been used to try to detect amphibole (Davidson et al., 2013), including Dy/Dy* and Dy/Yb (also in Fig. 15). Whilst amphibole fractionation should decrease Dy/Dy*, this ratio remains elevated. The trend for Dy/Yb remains flat, suggestive of clinopyroxene fractionation. Furthermore,

the trend of syn-subduction samples in REE multi-element space (Fig. 14) is flat, rather than the high LREE and 'spoon' shape often ascribed to amphibole.

With increasing evolution, many LFSE element contents remain low (Fig. 12). Biotite is often associated, with a high Rb distribution coefficient, K_d, of 1.9 in alkali basalts. It has high distribution coefficients for Sr and Ba (K_d values of 0.7 and 10 respectively), and can even host Th and U, with K_d values of 0.12 and 0.13 (Villement et al., 1981), which would explain the plateauing in their concentrations. Fractionation of biotite would also limit K contents and explain the plateau in K_2O, where fractionation of other minerals may increase it. Small amounts of biotite are suggested in fractionation models and vector modelling for fractional crystallisation of some trace elements (especially those mentioned above) resolve better when biotite is included. Unfortunately, both are inconclusive given the scatter of data. Previous studies have suggested that biotite is favoured over amphibole in fractionating assemblages

Table 3
Bulk rock trace element geochemistry, derived from XRF includes Ba, Ce, Cr, Cs, Ni, Pb, Y and Zr; those from ICP-MS are Hf, La, Nb, Nd, Ta, Tb, Th, U and Yb. All values in mg/kg^{-1}.

Sample	Ba	Ce	Cr	Cs	Dy	Eu	Gd	Hf	Ho	La	Lu	Nb	Nd	Ni	Pb	Pr	Rb	Sc	Sm	Sr	Ta	Tb	Th	Tm	U	Y	Yb	Zr
TU-19-248	533.20	17.27	37.63	1.87	3.375	1.906	4.715	1.468	0.676	13.741	0.282	3.00	17.099	7.72	9.14	3.778	72.98	42.35	4.396	850.29	0.000	0.784	1.661	0.279	0.833	20.68	1.775	45.08
TU-19-249	466.59	13.35	20.81	2.10	3.741	1.971	4.794	1.334	0.739	13.182	0.298	2.98	16.096	7.26	9.26	3.569	60.42	32.61	4.452	1044.12	0.000	0.926	1.431	0.336	0.674	22.95	2.025	36.70
NJ-17-02.1	413.5	30.2	242.9	2.0	4.180	1.554	5.193	2.851	0.872	13.689	0.305	5.0	18.096	143.8	3.5	4.089	41.8	24.8	4.788	909.8	2.475	0.680	1.510	0.544	0.546	22.0	2.233	78.1
NJ-17-02.2	178.5	17.7	235.0	2.0	3.412	1.168	3.641	1.923	0.714	6.962	0.287	3.7	10.306	58.0	3.7	2.174	58.5	32.3	2.949	688.3	1.464	0.572	0.711	0.440	0.322	17.4	1.780	53.5
NJ-17-03.2	492.0	11.4	39.2	1.9	3.414	1.195	3.524	1.623	0.744	6.151	0.296	2.6	9.638	18.5	2.6	2.013	21.7	29.4	2.885	517.5	0.197	0.552	0.639	0.468	0.319	17.8	2.055	39.1
VM-17-01.1	800.1	18.2	302.4	1.9	3.062	1.245	3.676	1.369	0.704	9.287	0.241	2.6	12.040	70.7	6.4	2.725	39.0	32.2	3.318	1114.2	0.119	0.529	1.166	0.388	0.550	14.4	1.739	24.5
VM-17-02.1	484.2	11.2	270.8	2.2	2.730	1.042	3.248	1.172	0.547	6.984	0.214	2.6	10.236	65.8	5.3	2.200	29.4	40.0	2.917	909.8	0.055	0.425	0.827	0.268	0.420	13.2	1.399	24.0
VM-17-04.1	1713.4	34.6	0.7	1.8	4.423	1.822	5.207	3.192	0.939	22.768	0.395	5.3	22.426	0.8	13.1	5.471	130.3	5.9	5.578	1197.1	0.302	0.717	3.810	0.520	1.573	20.7	2.626	84.3
VM-17-05	2137.3	35.3	0.4	1.9	6.708	2.183	7.505	4.156	1.542	37.352	0.615	7.8	30.620	0.7	16.5	7.669	142.0	6.6	6.458	1593.0	0.433	1.096	4.386	0.814	1.703	49.0	4.179	122.1
VM-17-06.1	1689.5	33.6	8.9	2.0	4.574	1.808	5.776	2.787	0.945	21.173	0.358	4.6	22.963	4.2	14.7	5.506	185.0	11.4	5.392	2115.2	0.252	0.775	3.239	0.522	1.321	22.2	2.755	62.2
VM-17-07	614.4	7.6	340.9	2.0	2.633	0.953	2.960	1.158	0.561	6.771	0.212	2.3	9.393	110.6	5.7	2.012	41.9	28.3	2.524	908.4	0.051	0.458	0.844	0.265	0.301	14.1	1.535	25.3
VM-17-09.1	1073.5	31.3	0.7	7.3	4.097	1.582	4.753	3.350	0.860	20.914	0.421	6.1	20.815	0.1	15.9	5.074	76.9	7.3	4.674	1426.6	0.317	0.681	3.456	0.462	1.453	22.1	2.641	100.9
FAD-50-01	72.25	10.35	22.15	1.72	3.210	1.004	3.341	1.417	0.685	5.042	0.265	4.04	7.734	0.82	4.62	1.861	22.26	39.79	2.539	173.51	0.847	0.751	0.459	0.313	0.263	21.96	1.910	77.81
FAD-50-02	101.57	17.21	0.66	1.69	4.048	1.218	4.443	1.500	0.893	9.497	0.300	7.05	15.467	0.66	2.92	3.474	35.19	19.86	3.955	70.29	0.541	0.824	0.742	0.414	0.410	25.45	2.179	132.75
RR-17-02.1	471.9	20.2	147.7	1.8	4.052	1.349	4.106	2.310	0.838	11.847	0.352	4.4	15.275	82.4	4.4	3.336	42.4	27.3	3.850	716.2	0.223	0.629	1.429	0.464	0.493	19.1	2.352	57.5
RR-17-03.1	474.6	17.4	172.7	1.9	4.052	1.424	4.395	2.224	0.879	11.477	0.335	4.4	14.834	94.0	4.7	3.316	32.6	27.3	3.630	718.2	0.233	0.656	1.387	0.487	0.477	21.1	2.287	55.6
TBH-004-18	236.15	7.50	226.15	1.89	2.352	0.899	2.537	1.031	0.508	5.590	0.222	2.67	8.262	58.87	6.42	1.758	44.23	39.89	2.362	395.81	0.240	0.466	0.673	0.224	0.315	13.85	1.324	34.21
TDH-004-06	251.11	6.59	142.25	1.94	2.454	0.895	2.414	0.989	0.512	3.152	0.244	2.37	5.389	44.75	1.93	1.191	18.07	48.91	1.883	427.11	0.240	0.580	0.283	0.249	0.296	16.98	1.517	32.61
TDH-004-16	321.05	14.86	175.29	1.94	2.805	1.174	2.754	1.225	0.579	6.337	0.237	2.68	9.185	66.75	2.89	2.186	35.94	32.79	2.814	576.42	0.353	0.538	0.785	0.275	0.412	15.00	1.364	35.55
TDH-004-17	660.99	24.20	89.61	1.91	3.249	1.453	2.961	1.982	0.639	12.198	0.276	4.66	14.792	31.49	4.40	3.509	40.59	21.32	3.325	961.71	0.314	0.530	1.494	0.239	0.596	15.40	1.550	52.28
FJ-19-01	595.30	33.09	16.16	1.94	4.146	2.017	5.812	0.994	0.808	17.10	0.317	3.19	23.29	3.55	7.34	5.43	99.43	19.76	5.730	1524.45	0.000	0.790	1.989	0.318	1.117	20.46	2.039	53.42
FJ-19-02	662.54	13.45	18.59	1.92	3.090	1.313	3.818	0.110	0.684	8.38	0.248	2.49	11.57	7.56	4.24	2.61	61.02	22.61	3.161	1152.39	0.000	0.536	1.421	0.265	0.690	16.00	1.614	27.32
FJ-19-03	553.53	20.67	17.22	1.91	3.638	1.775	4.907	0.591	0.753	15.98	0.292	2.79	19.17	3.25	8.16	4.49	79.90	16.29	4.758	1677.36	0.000	0.663	2.325	0.301	1.315	17.68	1.815	42.55
SBDD-0001-01	612.39	19.69	18.37	1.75	3.702	1.566	4.144	0.413	0.792	13.870	0.327	2.67	15.547	0.70	5.30	3.531	78.21	14.04	4.178	1721.76	0.240	0.751	2.974	0.374	1.649	21.71	2.075	60.19
SBDD-0001-04	750.76	19.79	9.33	1.85	3.547	1.682	3.341	1.225	0.564	15.512	0.274	2.56	15.587	0.74	14.47	4.009	119.56	6.34	3.382	2648.27	0.240	0.645	2.898	0.240	1.339	15.27	1.412	33.99
SBDD-0002-16	578.41	18.53	70.35	1.89	3.060	1.423	3.522	0.667	0.626	10.843	0.246	2.79	13.234	21.73	10.69	3.134	73.12	31.30	3.637	812.98	0.000	0.602	1.360	0.270	0.759	17.07	1.674	31.75
SBDD-0003-01	594.71	20.46	12.72	1.79	3.290	1.526	3.123	2.156	0.526	16.913	0.277	2.68	14.321	6.71	6.55	3.782	62.01	14.89	3.307	1481.93	0.240	0.593	3.734	0.235	2.066	16.52	1.509	65.85
SBDD-0003-08	915.73	19.70	4.89	1.85	4.026	1.779	4.761	1.018	0.794	11.480	0.327	2.37	17.543	1.30	8.47	4.002	89.83	12.00	5.343	1579.68	0.000	0.863	3.540	0.382	0.636	23.35	2.275	56.49
SBDD-0003-13	744.71	20.21	13.62	1.79	4.121	1.819	4.179	1.000	0.852	15.873	0.328	2.87	19.224	1.80	9.30	4.829	102.43	17.80	4.475	1502.17	0.240	0.724	3.849	0.326	0.999	20.61	1.855	62.35
SBDD-0003-29	671.35	34.73	9.30	1.84	3.492	2.054	4.946	2.724	0.675	23.232	0.354	2.68	20.819	0.74	15.71	5.106	101.68	14.74	5.087	1973.02	0.240	0.900	4.135	0.319	2.311	20.33	2.277	96.23
SBDD-0003–41	502.87	22.81	31.54	1.85	3.754	1.587	3.559	2.311	0.687	17.818	0.361	2.74	18.337	12.53	13.65	4.265	71.42	19.87	3.790	1304.59	0.000	0.668	3.504	0.291	2.245	17.86	1.867	62.01
SR-17-01.1	416.9	23.3	35.3	4.1	4.966	1.635	5.169	2.044	0.968	12.706	0.340	3.1	16.361	22.5	6.4	3.410	32.2	42.3	4.419	1004.0	0.087	0.777	1.767	0.441	0.880	24.1	2.454	48.3
SR-17-01.2	635.4	22.6	8.9	0.0	3.671	1.304	4.109	2.297	0.807	16.017	0.355	3.0	16.324	1.7	13.5	3.767	94.3	31.8	3.976	1262.9	0.125	0.624	3.509	0.411	1.650	20.6	2.278	68.2
SR-17-02.1	425.8	17.1	18.2	2.0	4.330	1.336	4.185	2.153	0.974	7.201	0.429	2.9	11.715	9.0	3.3	2.595	34.1	19.6	3.343	716.1	0.134	0.658	0.515	0.477	0.273	24.4	2.662	64.2
SR-17-02.2	884.4	68.9	106.0	0.1	6.978	3.797	11.336	3.741	1.271	33.951	0.396	3.5	46.719	24.6	15.1	10.284	77.9	31.9	12.358	2253.7	0.128	1.355	3.435	0.440	2.243	30.9	2.620	124.0
TU-19-009	563.70	23.98	9.30	1.87	3.867	1.794	4.080	2.381	0.664	17.727	0.342	3.39	20.318	0.71	8.87	5.112	99.75	12.64	4.497	1509.21	0.240	0.695	3.000	0.306	1.741	19.40	1.916	64.27
TU-19-010	615.22	24.42	13.28	1.89	3.554	1.961	4.688	1.816	0.667	18.092	0.324	3.39	19.039	0.73	33.64	4.901	89.40	13.70	4.501	1498.20	0.000	0.880	2.649	0.307	1.321	20.19	1.987	59.66
TU-19-035	650.17	22.54	15.55	1.90	3.864	1.811	4.528	1.787	0.792	18.043	0.330	3.30	20.648	0.74	10.82	5.225	93.66	14.71	5.223	1471.35	0.240	0.740	2.362	0.336	1.445	20.20	1.997	58.46
TU-19-036	612.43	30.25	9.46	1.87	4.098	1.714	4.572	2.192	0.814	17.775	0.358	3.37	22.198	0.72	11.46	5.353	92.96	14.54	4.769	1824.41	0.000	0.745	2.870	0.331	1.988	20.68	2.020	67.45
TU-19-040	663.46	24.59	43.77	1.91	3.999	1.952	4.548	2.324	0.684	19.205	0.359	3.32	21.169	1.27	8.16	5.067	77.39	15.29	4.674	1500.80	0.000	0.797	2.387	0.303	1.430	19.23	1.782	54.15
TU-19-048	646.79	28.88	12.57	1.88	4.080	2.101	4.338	1.854	0.723	20.039	0.340	3.40	22.274	0.73	11.01	5.123	97.65	15.60	5.076	1404.02	0.000	0.788	2.462	0.303	1.355	19.87	1.781	58.46
TU-19-049	671.21	21.31	31.00	1.89	3.761	1.973	4.611	1.926	0.676	19.248	0.332	3.08	20.421	0.74	9.68	4.967	99.25	16.11	4.733	1389.09	0.000	0.838	2.102	0.298	1.139	19.08	1.855	47.91
TU-19-050	654.57	24.06	11.12	1.90	3.349	2.021	4.680	1.652	0.665	16.754	0.296	3.20	18.007	0.74	8.39	4.608	96.41	15.45	4.650	1557.48	0.000	0.854	1.939	0.297	0.959	18.84	1.789	46.22
TU-19-051	630.85	21.64	6.94	1.88	4.034	1.948	4.609	2.055	0.786	17.975	0.338	3.32	22.046	0.74	8.61	4.995	92.10	14.41	5.085	1630.85	0.000	0.705	2.167	0.294	1.354	19.07	1.893	51.21
TU-19-055	704.03	20.52	15.26	1.83	3.058	1.693	3.985	1.828	0.578	20.146	0.281	3.52	17.249	0.66	13.43	4.493	125.87	8.91	3.875	1607.77	0.000	0.724	2.567	0.276	1.688	16.18	1.673	62.65
TU-19-056	981.77	25.01	8.44	1.86	3.962	2.105	4.987	2.366	0.804	22.819	0.379	2.97	24.319	0.68	11.91	5.984	133.79	7.93	5.274	1763.93	0.000	0.808	2.744	0.355	1.961	19.96	2.217	83.71
TU-19-086	882.57	12.30	1.30	1.83	2.027	1.420	2.293	2.431	0.421	10.991	0.229	4.60	9.875	0.61	18.29	2.482	139.93	6.76	2.534	1445.23	0.240	0.383	3.816	0.206	2.391	12.07	1.244	158.86
TU-19-089	189.14	8.91	−3.81	1.81	1.098	0.734	1.138	0.455	0.195	5.644	0.089	3.56	5.169	0.54	8.67	1.297	134.70	4.95	1.165	247.03	0.000	0.200	0.995	0.074	0.601	7.02	0.499	76.11
TU-19-101	668.27	53.04	117.04	1.89	6.173	2.558	8.966	2.926	1.224	37.928	0.606	4.41	41.186	0.68	12.68	11.007	138.15	7.03	9.222	1198.95	0.240	1.542	9.547	0.628	2.882	39.65	4.136	137.78
TU-19-112	468.82	21.33	6.69	1.93	3.512	1.715	4.191	1.355	0.656	15.334	0.249	3.12	19.745	0.71	6.19	4.601	66.75	18.75	4.700	1108.98	0.000	0.635	1.466	0.269	0.946	16.73	1.540	45.21
TU-19-113	606.42	24.94	15.18	1.92	3.617	2.097	5.185	1.649	0.688	17.367	0.265	3.19	21.013	2.76	5.74	4.581	75.41	22.61	5.365	1650.62	0.000	0.964	1.711	0.306	0.736	20.15	1.862	50.00
TU-19-120	628.99	17.55	15.74	14.25	3.610	1.882	4.140	1.553	0.684	15.878	0.288	2.64	18.650	1.19	10.61	4.672	78.86	18.37	4.361	1735.96	0.000	0.705	1.646	0.276	0.844	16.80	1.555	31.00
TU-19-128	446.64	46.47	34.54	1.90	8.183	2.921	9.858	1.540	1.493	32.507	0.684	3.82	41.462	11.60	20.19	10.106	100.12	22.80	10.096	1124.28	0.000	1.730	7.319	0.636	1.392	44.72	3.778	88.02

Table 3 (*continued*)

Sample	Ba	Ce	Cr	Cs	Dy	Eu	Gd	Hf	Ho	La	Lu	Nb	Nd	Ni	Pb	Pr	Rb	Sc	Sm	Sr	Ta	Tb	Th	Tm	U	Y	Yb	Zr
Sample	Ba	Ce	Cr	Cs	Dy	Eu	Gd	Hf	Ho	La	Lu	Nb	Nd	Ni	Pb	Pr	Rb	Sc	Sm	Sr	Ta	Tb	Th	Tm	U	Y	Yb	Zr
TU-19-159	1138.98	7.67	9.53	1.78	0.594	0.927	0.653	0.350	0.105	1.642	0.031	7.62	2.904	0.57	3.19	0.562	148.02	10.54	0.758	526.15	0.240	0.108	0.221	0.038	0.287	3.40	0.216	123.93
TU-19-160	653.17	22.75	12.91	1.89	4.042	2.306	5.101	1.884	0.803	17.140	0.341	2.81	20.877	0.76	9.30	5.040	58.13	18.32	5.706	1334.18	0.000	0.889	2.010	0.365	1.084	20.21	2.052	47.74
TU-19-178	119.32	7.94	46.09	1.78	3.826	1.202	3.261	0.617	0.822	3.657	0.371	2.65	7.832	11.23	19.22	1.609	51.22	38.43	2.722	267.55	0.000	0.776	0.172	0.375	0.492	23.56	2.291	73.59
TU-19-210	636.63	27.85	17.93	1.90	3.945	1.982	4.901	1.570	0.811	18.183	0.284	3.07	23.389	7.93	4.74	5.429	75.33	22.62	5.745	1456.70	0.000	0.803	1.558	0.317	1.019	21.23	1.720	49.13
TU-19-213	640.15	26.81	12.20	1.91	4.285	1.875	4.549	1.993	0.819	17.461	0.340	3.03	23.244	10.39	7.72	5.196	76.47	15.87	5.001	1542.10	0.000	0.754	2.057	0.320	1.154	20.56	1.960	48.77
TU-19-238	377.49	25.91	78.70	1.97	4.188	2.210	5.530	2.137	0.842	19.535	0.345	3.12	25.285	9.05	11.39	5.880	49.35	33.03	6.459	1148.70	0.000	0.807	2.212	0.341	1.389	22.53	1.881	58.75
TU-19-250	256.82	15.99	31.47	1.86	3.744	1.511	4.028	1.826	0.685	14.739	0.304	2.64	16.623	6.37	7.77	4.150	24.66	22.70	4.113	1107.73	0.000	0.830	0.907	0.308	0.772	20.22	1.876	54.79
TU-19-251	544.83	16.08	25.36	1.95	3.638	1.665	3.840	0.904	0.722	12.277	0.267	2.02	17.103	14.57	4.79	3.756	62.62	32.47	4.288	1155.40	0.000	0.688	0.918	0.267	0.357	18.17	1.621	17.88
TU-19-252	588.22	26.13	23.12	1.92	4.075	1.931	4.549	2.176	0.709	20.303	0.370	3.49	21.168	0.73	17.43	5.325	96.86	18.20	4.694	1131.68	0.000	0.814	2.813	0.309	1.611	19.97	1.987	66.11
TU-19-253	589.85	21.29	53.09	1.99	4.328	2.008	4.389	1.953	0.812	18.471	0.340	3.30	23.517	9.03	11.30	5.429	92.36	29.20	5.108	1306.77	0.000	0.717	2.241	0.299	1.276	19.79	1.723	52.44
TU-19-254	622.96	26.93	14.68	1.99	4.167	1.955	4.522	1.955	0.802	16.483	0.334	2.94	21.779	9.29	10.88	4.978	95.78	33.64	5.004	1308.56	0.000	0.786	2.044	0.300	1.176	19.71	1.894	50.34
TU-19-255	624.5	30.8	20.3	2.1	4.353	1.845	5.646	2.353	0.886	16.405	0.337	2.7	20.294	5.2	4.3	4.747	70.8	21.4	5.473	1453.2	0.395	0.737	2.301	0.517	1.054	21.3	2.211	62.2
TUDDH-398a	514.8	19.3	20.1	2.1	3.111	1.154	3.755	1.504	0.608	10.526	0.256	3.0	13.447	14.2	2.0	3.017	65.3	25.0	3.665	1399.9	0.169	0.496	1.480	0.246	0.779	18.8	1.747	42.9
TUDDH-398b	809.2	31.3	16.2	2.1	4.487	1.818	5.744	2.377	0.953	18.479	0.388	3.1	22.950	0.0	9.0	5.111	97.7	15.7	5.497	1702.3	0.354	0.771	2.646	0.500	1.405	21.0	2.478	52.6
TUDDH-408a	691.8	21.3	48.8	2.1	4.446	1.796	5.419	2.334	0.854	18.368	0.335	3.2	21.211	1.1	9.8	4.854	98.6	14.6	5.274	1532.5	0.268	0.720	2.547	0.516	1.370	19.4	2.286	51.9
TUDDH-415	683.4	42.0	40.2	2.2	3.868	1.600	4.885	1.947	0.771	14.735	0.298	3.1	17.930	0.9	16.2	4.136	111.2	18.8	4.759	821.8	0.224	0.642	2.795	0.461	1.122	18.3	2.203	53.3
TUDDH-427	599.2	23.9	41.1	2.0	0.788	0.318	1.043	0.450	0.157	2.752	0.057	3.7	3.513	13.7	13.9	0.756	103.6	23.5	1.044	1022.4	0.006	0.134	0.806	0.000	0.139	24.3	0.394	83.0
TUDDH-437	630.6	26.0	9.0	0.2	4.108	1.650	5.027	2.587	0.790	18.173	0.373	3.8	20.419	0.5	13.1	4.823	106.8	14.0	4.732	1397.7	0.241	0.687	3.295	0.462	1.787	18.9	2.396	69.1
TUDDH-456	1655.1	23.5	37.7	2.3	2.692	1.301	3.640	2.569	0.590	18.782	0.202	9.5	16.234	0.4	9.3	4.186	218.8	13.3	3.766	783.1	0.609	0.463	2.479	0.335	0.812	14.5	1.570	59.4
TUDDH-463b	752.0	26.3	1.9	1.9	3.351	1.392	4.055	1.549	0.716	20.616	0.284	2.8	18.635	0.5	19.7	4.603	129.0	8.1	4.136	1475.6	0.152	0.570	1.709	0.352	1.031	15.6	1.922	30.6
TUDDH-469	556.69	11.55	12.47	1.76	5.385	1.451	5.133	0.660	1.193	8.50	0.529	2.94	12.49	3.47	3.10	2.73	21.05	19.60	3.684	692.30	0.000	0.840	0.779	0.524	0.385	32.05	3.157	53.17
LL-17-01.1	565.18	6.91	11.26	1.77	5.197	1.418	5.119	0.715	1.205	8.31	0.556	2.77	12.63	2.51	3.87	2.62	21.44	22.59	3.605	684.31	0.000	0.834	0.766	0.510	0.407	32.39	3.155	53.30
FJ-19-04a	547.51	6.72	8.42	1.75	3.477	1.144	3.330	0.655	0.769	6.14	0.370	2.99	8.43	1.58	3.96	1.89	19.67	18.71	2.408	741.90	0.000	0.540	0.746	0.364	0.356	19.65	2.192	55.26
FJ-19-04b	713.7	31.7	10.1	0.3	3.883	1.536	4.456	2.532	0.829	21.814	0.343	2.6	18.778	1.1	9.0	4.569	57.8	10.7	4.208	1228.2	0.115	0.619	4.638	0.404	2.321	19.8	2.249	76.8
FJ-19-05	595.7	25.2	20.8	2.0	3.543	1.239	3.896	3.222	0.737	16.943	0.344	4.1	16.652	4.1	3.8	4.023	23.6	15.2	3.791	515.8	0.173	0.554	2.215	0.361	0.768	20.7	2.153	115.0
MQ-17-01.1	261.5	33.0	23.0	1.8	4.042	1.581	4.739	1.945	0.816	14.219	0.298	3.3	18.436	13.2	4.6	4.004	15.0	20.9	4.516	613.1	0.106	0.680	1.503	0.372	0.666	19.9	2.059	60.3
NJ-17-01.1	39.9	5.5	26.8	2.1	4.009	0.992	3.517	1.528	0.874	2.505	0.341	2.9	6.764	3.0	0.7	1.263	2.7	38.5	2.307	219.3	0.585	0.564	0.130	0.514	0.058	22.0	2.472	46.9
NR-17-01.3	247.9	14.1	12.0	1.8	4.853	1.164	4.576	4.088	1.113	8.027	0.475	3.6	12.001	1.7	1.2	2.658	12.7	21.5	3.499	261.6	0.677	0.760	1.431	0.665	0.582	28.4	3.263	114.9
NR-17-01.4	53.7	2.6	0.7	1.8	4.747	1.289	3.355	0.861	0.972	1.862	0.554	2.3	6.295	0.9	0.1	1.105	2.9	43.1	2.439	153.6	0.000	0.791	0.118	0.476	0.066	28.9	3.011	30.6
BB-17-01.2	37.2	7.4	−6.8	1.8	4.382	1.267	3.290	0.447	0.923	1.698	0.447	2.4	5.858	0.7	0.4	1.001	2.3	30.1	2.497	143.1	0.000	0.851	0.081	0.462	0.039	27.3	2.725	29.5
BB-17-01-1	114.72	7.08	196.25	1.82	3.873	1.105	3.692	0.537	0.855	4.61	0.343	2.82	9.30	44.74	1.66	1.99	9.93	41.20	2.747	339.97	0.000	0.608	0.321	0.360	0.270	21.77	2.124	60.92
FJ-19-06ai	120.46	9.21	212.43	1.83	3.925	1.168	3.923	0.596	0.920	4.42	0.338	2.57	9.35	43.52	0.73	1.93	10.26	43.10	2.811	336.79	0.000	0.622	0.409	0.412	0.292	21.36	2.123	60.33
FJ-19-06aii	193.56	11.26	169.04	1.77	4.140	1.204	4.028	1.030	0.937	4.70	0.379	2.75	9.56	43.30	1.58	2.04	16.68	30.47	2.946	350.17	0.000	0.671	0.448	0.407	0.322	23.94	2.380	71.06
FJ-19-06bi	190.47	7.13	156.26	1.76	4.028	1.141	3.981	0.960	0.943	4.86	0.369	2.69	9.67	44.35	1.74	2.01	17.06	30.75	2.847	351.32	0.000	0.649	0.447	0.405	0.313	23.89	2.317	71.10
FJ-19-06bii	137.06	9.92	54.49	1.75	3.476	1.049	3.447	1.159	0.753	6.94	0.328	3.05	10.35	20.46	3.01	2.41	14.84	25.06	2.651	428.10	0.000	0.561	0.805	0.331	0.529	17.93	1.995	75.41
FJ–19-06c	223.84	16.09	18.84	1.90	5.508	1.514	5.432	3.012	1.273	6.40	0.538	3.69	13.61	0.75	0.74	2.95	18.23	30.61	3.982	735.62	0.000	0.893	0.467	0.538	0.188	28.42	3.348	122.00
FJ-19-07	61.1	2.6	5.6	0.4	3.254	0.780	2.100	1.038	0.705	1.281	0.365	2.1	3.887	0.9	0.7	0.735	6.1	29.1	1.730	178.1	0.000	0.550	0.081	0.348	0.052	19.6	2.031	27.6
KV-17-02.1	78.8	10.7	15.1	0.8	4.144	1.222	3.742	1.051	0.860	8.329	0.441	3.5	11.731	1.0	0.2	2.666	11.2	37.1	3.359	247.6	0.000	0.862	0.647	0.421	0.212	25.7	2.461	69.7
NR-17-01.1	139.3	15.5	12.9	2.1	5.649	1.389	5.136	2.972	1.223	7.464	0.534	3.5	13.439	3.1	2.3	2.729	15.9	23.8	3.765	500.5	0.196	0.844	0.728	0.643	0.309	29.6	3.485	85.0
WR-17-01.1	8.0	0.5	30.9	0.2	0.681	0.241	0.477	0.000	0.144	0.221	0.088	2.1	0.707	9.4	0.7	0.127	2.4	25.1	0.317	140.1	0.000	0.118	0.011	0.071	0.002	4.8	0.506	
WYR-17-01.1	1138.98	7.67	9.53	1.78	0.594	0.927	0.653	0.350	0.105	1.642	0.031	7.62	2.904	0.57	3.19	0.562	148.02	10.54	0.758	526.15	0.240	0.108	0.221	0.038	0.287	3.40	0.216	123.93

Fig. 12. Bivariate plots of trace element contents in ppm against SiO$_2$ wt%. Darker/ more opaque dots represent primary data whilst paler dots show literature data. Where error bars are greater than the size of the dots, vertical error bars are in the top right of the individual graph.

under drier and more K-rich conditions such as the Dariv Igneous Complex, Western Mongolia (Bucholz et al., 2014). Of the two, the dominant control over biotite crystallisation as a high temperature phase is the extent of K-enrichment: increased K leads to biotite

becoming favourable. Whilst the low-K bulk composition of subduction samples suggests this is unlikely, biotite *is* found in some subduction samples as a phenocryst.

Modelled fractionating assemblages have bulk compositions similar
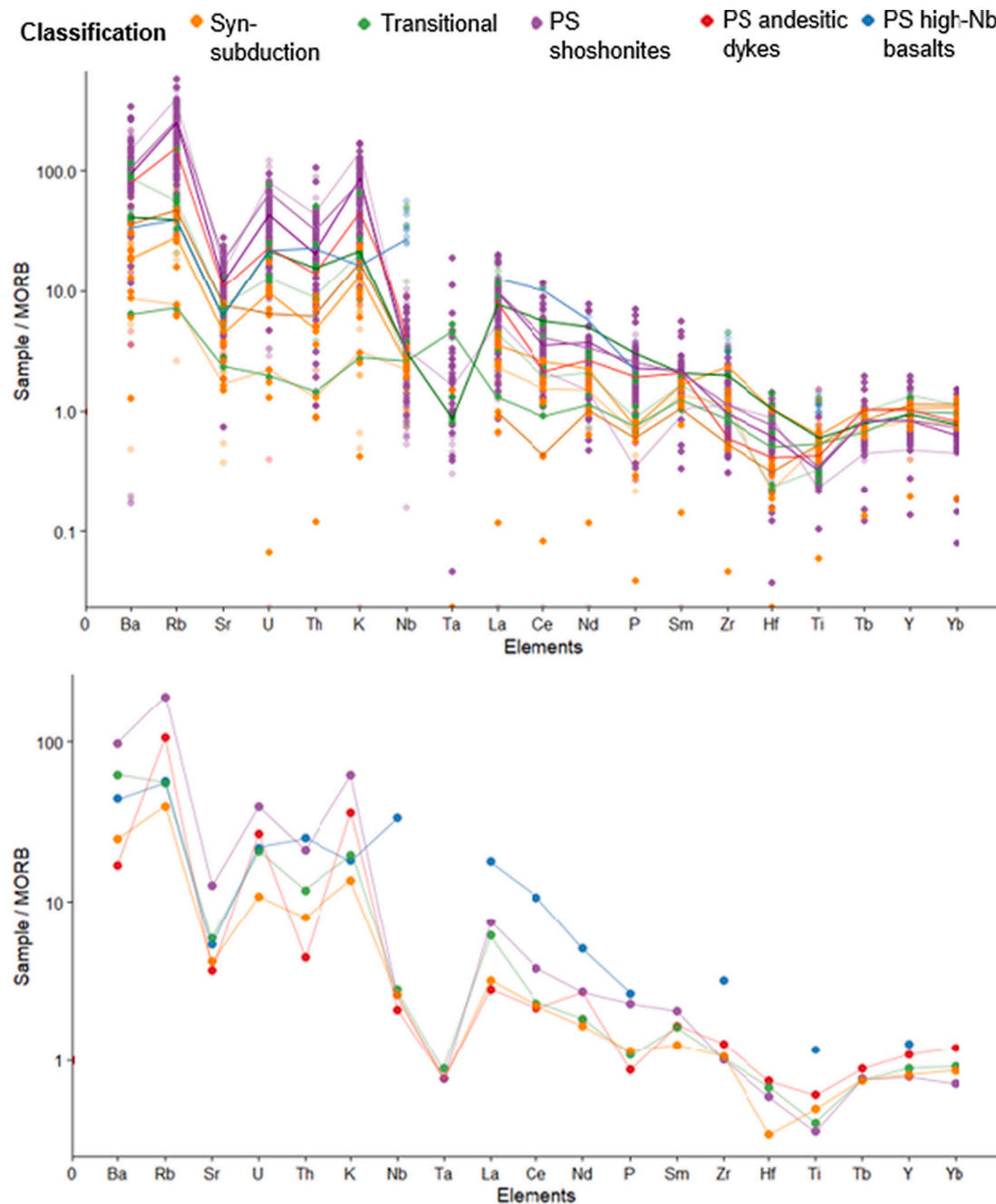
Fig. 13. Multi-element plot showing whole-rock trace element concentrations of samples normalised to MORB (using values from Klein (2004)). Top diagram shows data for all samples, whereas the bottom diagram shows the median values, as calculated using all data, inclusive of that derived from the literature. For syn-subduction, transitional samples, and post-subduction shoshonites, 3 representative samples have lines connecting the analyses. Only one representative line for the post-subduction andesitic dykes and post-subduction high-Nb basalts have been added, as there are far fewer analyses. Variations of colour have been used for lines so that where there is a gap in data for Ta, the lines can be traced across.

to *syn*-subduction rocks, which would explain gentle bivariate trends lacking strong inflections. This has important implications when considering models for mineralisation, as it is the ability of amphibole-rich cumulates to function as a sponge for metals and to store >20% of the water from arc flux (Davidson et al., 2007) that may aid Au and Te productivity in later magmas (Richards, 2009). Amphibole-poor litho-spheric cumulates would likely be a poorer store for water and metals, and inconsistent with the metallogenic models of post-subduction min-eralisation that require these enriched sources.

3.1.2. Source

Only once fractionation is accounted for can the source be consid-ered. Less evolved syn-subduction rocks across the Fijian arc have a mineralogical and geochemical signature that is consistent with flux melting within the mantle wedge. The primary mantle wedge at arc-inception was 'Pacific' in isotopic character (Todd et al., 2012), and the mantle is argued to have contained variably enriched components (Gill, 1984; Todd et al., 2012). Despite ratios such as those plotted against SiO_2 in Fig. 15 being much lower than those for post-subduction shoshonites (Ba/La <50, Rb/Zr <1), depleted mantle sources (as defined by normal MORB) have much lower Rb/Zr, Th/Zr, etc, than is seen in
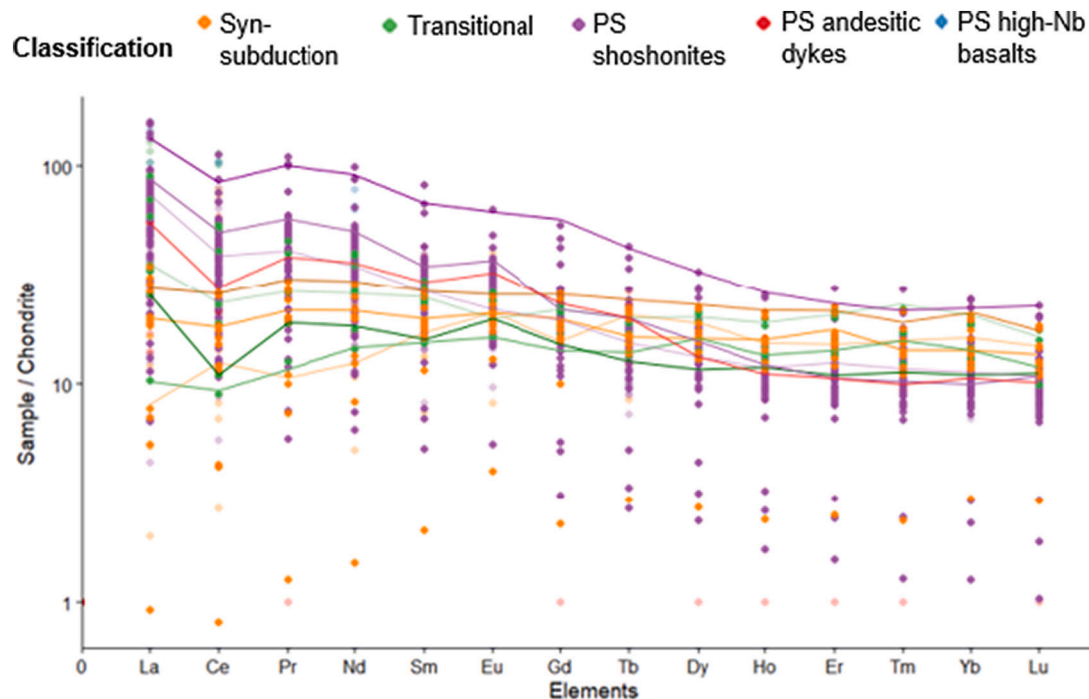
Fig. 14. Multi-element plot showing REE contents of samples, with values normalised to chondrite (using values from McDonough and Sun (1995). Again, for syn-subduction, transitional samples, and post-subduction shoshonites, 3 representative samples have lines connecting the analyses. Only one representative line for the post-subduction andesitic dykes and post-subduction high-Nb basalts have been added, as there are far fewer analyses.

syn-subduction suites. There is a clear enrichment in LILE compared to MORB as shown in Fig. 13, hence characteristics such as low K and low LREE cannot be explained by a depleted mantle source.

3.2. Transitional and post-subduction petrogenesis

3.2.1. Fractionation

Transitional samples show many similarities to syn-subduction rocks in bivariate space and REE space (Fig. 14). It is therefore assumed that fractionation pathways for the two groups are similar.

Whilst post-subduction shoshonites show LILE enrichments at low SiO$_2$, Fig. 13 shows steeper trends for more evolved post-subduction shoshonites, as samples contain increasingly extreme enrichments compared to syn-subduction samples from Fiji, and global arc compositions (tholeiites and calc-alkaline) more generally (Schmidt and Jagoutz, 2017). The simplest way to explain evolution trends is via fractionation. Least squares regression modelling was attempted for post-subduction shoshonites to constrain the assemblage, but as Σr^2 values (the sum of the squares of the misfits in the regression) were rarely less than 5, it was considered that the model does not resolve. When considering fractionation qualitatively, a broadly similar fractionation assemblage to that for syn-subduction is suggested. Fractionation of clinopyroxene dominating over olivine in an already potassic parental magma is thought to be the cause of the rapid increase in K$_2$O at Vatukoula (Rogers and Setterfield, 1994). This is an attribute apparently common to many potassic suites e.g., the Italian Province (Appleton, 1972), though wall-rock interaction is also cited as a potential trigger at the Roccamonfina Volcano. On the contrary, it has been suggested that extensive olivine fractionation may be responsible for low Ni/Mg ratios at Tavua, a feature which extends across shoshonitic centres (Gill & Whelan, 1989), though as outlined in the mineralogy, no olivine is observed at Tuvatu. In contrast to the syn-subduction fractionating assemblage, increasing Al$_2$O$_3$ and Sr suggest that plagioclase is not an important fractionating phase in the shoshonites; the increasing Al$_2$O$_3$ may instead point to some accumulation of plagioclase in the final whole rocks. Ratios in Fig. 15 such as Sr/Y, La/Yb and Dy/Yb are higher than

those achieved during subduction, and reflect a mix of feldspar accumulation, and limited fractionation of MREE and HREE. Fig. 14 shows REE curves inconsistent with significant amphibole fractionation.

3.2.2. Source of post-subduction shoshonites

Syn- and post-subduction magmas have comparable major and trace element characteristics at low silica contents. It has long been suggested that it is possible to extract melts during post-subduction with similar characteristics to syn-subduction melts if the source was modified during subduction (Harris et al., 1986). Literature Pb isotopic data is similar across subduction and post-subduction, suggesting an enriched source for both early-arc rocks (Todd et al., 2012) and post-subduction shoshonites (Leslie et al., 2009). Broadly similar Sr and Nd isotope data also occur through subduction up to 3 Ma (Gill, 1984). At this point, εNd values more typically range between 4 and 5 as opposed to 6 and 9 during syn- and post-subduction. This suggests the same, though perhaps slowly evolving, mantle source is being exploited throughout the transition, despite changes in geochemistry. Furthermore, radiogenic isotopes are similar to other circum-Pacific arcs (Rogers and Setterfield, 1994).

Transitional rocks have a similar mineralogy to syn- and post-subduction shoshonite samples, and similar geochemistry to syn-subduction samples. It is interesting that even those forming contemporaneously with, and from volcanoes adjacent to, shoshonitic centres do not show high enrichment ratios in Fig. 15, despite apparent mixing between magmas (Gill & Whelan, 1989). This suggests that if the enrichment is a source characteristic, the source contains small scale heterogeneities. (Schmitt et al., 2006).

3.2.2.1. Degree of melting. Gill and Whelan (1989b) suggest that differences between the post-subduction shoshonites and contemporaneous transitional rocks are caused by variable percent melting of the same source; shoshonites being produced via low degree (~4%) melting as opposed to 16% for calc-alkaline to tholeiitic post-subduction rocks. This is supported by comparable ratios of HFSE to each other (e.g., Nb/Zr, Y/Zr, Zr/Hf, Y/Nb) and to HREE (e.g., Y/Dy, Zr/Yb) across rock
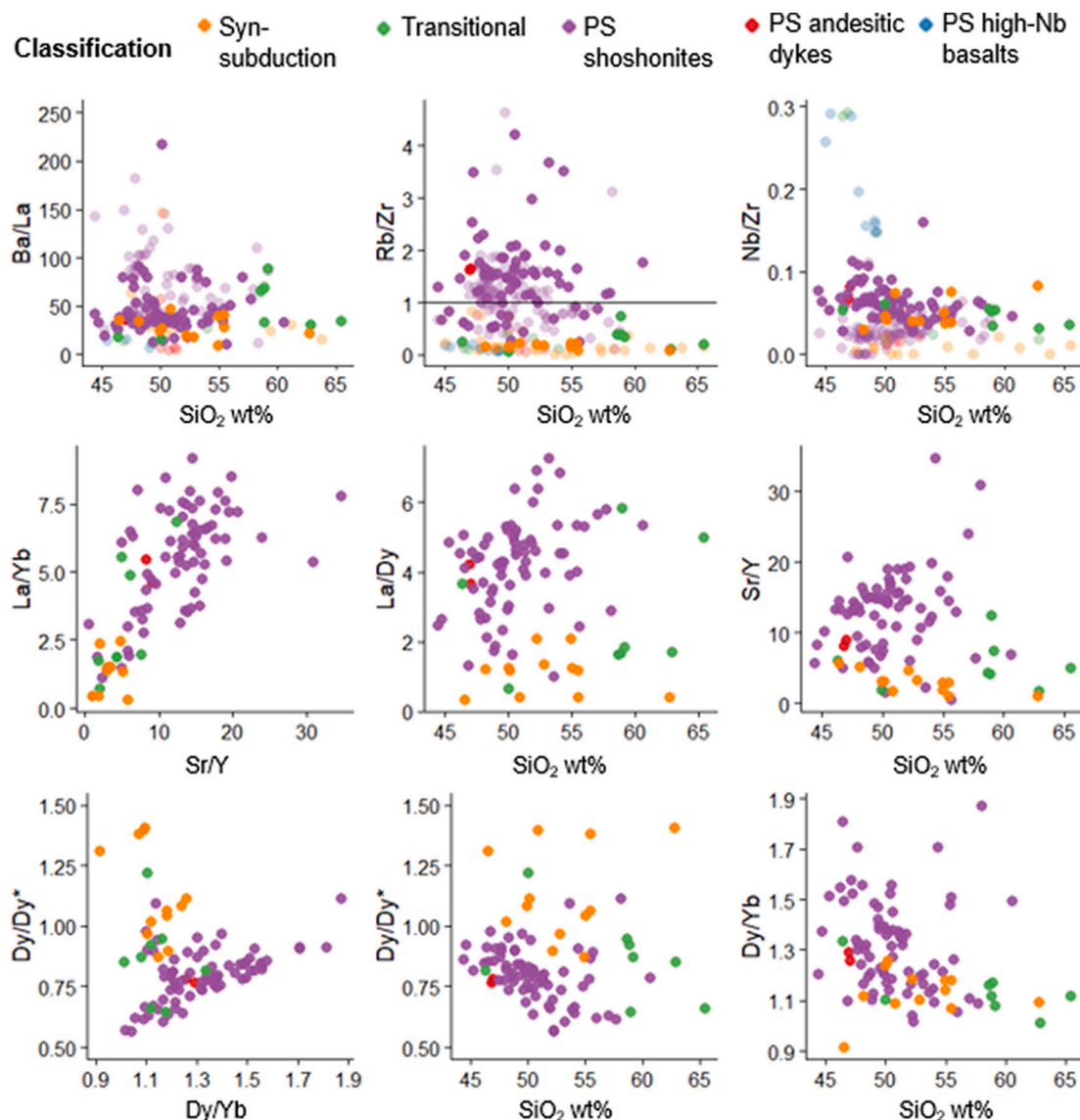
Fig. 15. Graphs showing trace element ratios often used when determining source enrichment (Sr/Zr, Rb/Zr) and melting regime (Nb/Zr). Patterns suggestive of fractionation (Sr/Y, La/Yb, La/Dy, Dy/Yb and Dy/Dy*) use chondrite normalised data. Dy/Dy* uses equation from Davidson et al. (2013).

types. The initial enrichment in Rb, Ba and K_2O at low silica contents within shoshonites could also suggest low degrees of partial melting.

However, low Nb/Zr ratios imply that low degree partial melting can be ruled out. The general depletion of Nb and Ta is often caused by higher degree melting under fluid flux, allowing fluid mobile elements to become enriched whilst the Nb-Ta signal stays relatively low. This is more in line with Rogers and Setterfield (1994), who suggest that high melt-fractions (up to 20%) of an enriched mantle source may have formed the Tavua Volcano, based on major element abundances (e.g., low Na_2O, high CaO), although this then requires another mechanism for the addition of LILE.

3.2.2.2. Mantle source. In addition to different element ratios, post-subduction shoshonites are distinct on Harker diagrams (Fig. 11, Fig. 12) where they show enhanced subduction signatures. When primitive arc melts across the world are compared (Schmidt and Jagoutz, 2017), these post-subduction shoshonites meet criteria for mantle-equilibrium. Nonetheless, multi-element diagrams show that they have a distinct chemistry in comparison to arc magmas, often reaching anomalous concentrations of LILE and producing a more prominent Nb-Ta depletion. These 'extreme' subduction signals occur

despite the change in tectonic regime, which may be expected to reduce subduction influence. That said, subduction flipping likely occurred sometime between 10–8 Ma, exposing the Vitiaz mantle wedge to Vanuatu subduction once the Vanuatu slab reached sufficient depth, possibly only shortly before arc migration isolated Fiji at ~5Ma. Whilst many suggestions exist for the formation of these shoshonites, most require a mantle source more strongly enriched in LILE than is typically observed across arcs (Gill & Whelan, 1989; Rogers and Setterfield, 1994). A source enrichment is suggested in Fig. 15, where Ba/La and Rb/Zr are especially high. Work by Leslie et al. (2009) suggests that although significant spatial heterogeneities in the background fertility of mantle affects the sensitivity to subduction contribution, it is the additions themselves that are responsible for the LILE enrichments.

3.2.2.3. Subduction contributions. Subduction contributions have variably been suggested to include slab melts, slab fluids, and sediment contributions to explain the distinct chemistry. Depletions of Nb and enrichments of K, Rb, Ba, Sr and LREE as observed in Fiji have been attributed to slab melts elsewhere, including in the Finero Complex, Italy (Zanetti et al., 1999), and Sierra Nevada and the Western Mexico Volcanic Belt (Bucholz et al., 2014). Whilst slab surface temperatures

beneath Fiji during early subduction make a significant slab melt contribution unlikely (Todd et al., 2012), this is not constrained during later stages.

Slab fluids from down-going oceanic crust have long been considered major transporters of K, Ba, Sr, and Rb (Anderson et al., 1978) and these contributions have been considered as a possible cause for enrichments at Tavua. This is supported by the lack of correlation between these elements and Th/Ta ratios (Rogers and Setterfield, 1994), although an unusually large input would be required. Breakdown of amphibole releasing high-K fluids into the mantle wedge has been suggested in Baja California (Saunders et al., 1987). However, there melts have high K/Rb and K/Th ratios; a function of mantle exhausting Rb and Th during subduction, and then breakdown of amphibole releasing high K/Rb and K/Th fluids.

Sediment contributions can become highly potassic with increasing pressure (Schmidt et al., 2004), exacerbating the potassic nature of later magmas and producing a much less hydrous subduction signal. A high sediment input can increase alkalis and Th contents (Plank and Langmuir, 1998), both of which are greater in Fijian post-subduction shoshonites. Sediment melting is also proposed by Leslie et al. (2009). However, whilst Ba, Rb, and Sr all reach elevated levels, Th is only elevated relative to syn-subduction samples; in comparison to arc rocks elsewhere Th and U remain low, suggestive of a lower sediment contribution in line with Rogers and Setterfield (1994) who suggest sediment contributions <4%. There is also no negative Eu anomaly in Fig. 14, and Pb isotope data in Gill (1984) indicate sediment input is precluded as shoshonites and arc lavas are indistinguishable. Logically, it seems unlikely that sediment contribution could vary so significantly both temporally and spatially.

If subduction contributions are responsible for the distinct geochemistry, the question remains as to how non-contemporaneous post-subduction shoshonites show such extreme subduction signals and enrichments when syn-subduction samples do not. Active subduction beneath Fiji had ceased (Begg and Gray, 2002), and whilst seismic evidence indicates a remnant slab beneath Fiji five to eight million years ago (Chen and Brudzinski, 2001), the regime then was extensional (Begg and Gray, 2002; Hathway, 1993). Therefore, it is unlikely that post-subduction decompression melting would be able to access any direct contribution from Vitiaz subduction.

3.2.3. Cumulates

Syn-subduction and post-subduction suites require crystal fractionation to evolve. Therefore, it follows that there must, somewhere, be crystal accumulations. The role of these cumulates is discussed here for three reasons.

The first is their implied importance in the formation of deposits such as Vatukoula and Tuvatu. Given their proposed storage of elements such as Au, Ag and Te, and volatiles (Davidson et al., 2007), their ability to impact bulk magmatic chemistry of these melts should also be considered. Elsewhere in the world, amphibole and/or clinopyroxene cumulates are an important lower crustal lithology (Medard et al., 2006; Schiano et al., 2000), with examples found in dykes in SE Europe, East Sunda Arc and Sierra Nevada (Georgiev et al., 2009; Turner et al., 2003). Whilst metasomatised lithospheric mantle is favoured in some models, it should be noted that arc cumulates can be relatively mantle-like themselves, such as those in Kohistan containing garnet-pyroxene-amphibole-plagioclase (Jagoutz et al., 2011).

Second, it seems logical that post-subduction melts would have to pass through subduction-formed residues or cumulate assemblages within the crust. A relatively low velocity layer in the mid-crust at roughly 11–16 km below Fiji is ascribed to crustal rocks with intermediate compositions of tonalite or andesite (Chen et al., 2019), further supporting this notion. This composition is also consistent with fractionation assemblages reported to remelt and form shoshonites elsewhere (Georgiev et al., 2009). However, fractionating the same minerals which are present within later magmas makes AFC difficult to monitor,

as assimilating material is unlikely to have a chemically distinct signature.

Third, is that cumulates are a viable source for creating the peculiar characteristics of post-subduction shoshonites. As explained above, models for the differences seen across post-subduction rocks often require differences in mantle composition (Leslie et al., 2009) or differences in melt fraction (Gill & Whelan, 1989) on a scale of 10–15 km. These small-scale differences may be more easily explained by the presence of cumulates with heterogeneous mineral assemblages and distribution through the crust. Previous literature precluding them suggest that crustal assimilation is not enough to drive trends (Gill & Whelan, 1989), or that isotope data rule out significant interaction with radiogenic crust (Leslie et al., 2009), though this is often based on assumptions on the composition of assimilating crust.

Petrography and fractionation models suggest that amphibole is not an abundant mineral in the Fijian lithosphere, and elevated Rb, Th, and U are inconsistent with an amphibole-rich source, or amphibole assimilation. However, elevated contents of Th and U, as well as Ba, Pb, Rb, and Sr in post-subduction rocks could be caused by the presence of biotite in cumulates. This would support the extreme enrichment of Ba compared to Rb, as during biotite crystallisation from alkali basalts Ba is 1.5–13 times more compatible than Rb (Villement et al., 1981). Whilst *syn*-subduction melts may have contained too little K to crystallise biotite, it is seen as a phase in a few subduction samples. It is possible that biotite formed as mesostatic pockets in the interstices trapped between the other, low-K phases when the residual liquids had developed locally high K concentrations. These may then melt preferentially to feed into the shoshonites, providing a pre-enrichment mechanism for their formation. The resulting trace element systematics are difficult to model given the non-liquid compositions of the shoshonites. Qualitatively, some trace element vector modelling of AFC appears to suggest that addition of biotite could drive the extreme trends observed in some LILE. Therefore, we suggest that it is the assimilation or melting of biotite from the lithosphere, and likely from cumulates in the crust, that confer the distinctive chemistry of the Fijian shoshonites.

Models for the formation of ultrapotassic and shoshonitic rocks often invoke a lithospheric mantle, modified by infiltration of veins of pyroxene, phlogopite and/or amphibole (Foley, 1992; Holwell et al., 2019). All the "vital ingredients" for this process would be expected in the cumulate pile in the lowermost arc crust, and so the productive zone for the post-subduction potassic melts spans the metasomatised lithospheric mantle into the lower crust. Formation of the labile components (biotite) by fractionation, rather than through in-situ cooling of an infiltrating low degree partial mantle melt to phlogopite-rich veins (as per Foley (1992)) would be more consistent with the low Nb in the shoshonites. Micas are good reservoirs for Nb and should faithfully record Nb-enrichment in their parent melt (Ewart and Griffin, 1994; Ionov et al., 1997) – thus the sources for the relatively Nb-poor Fijian shoshonites need micas formed from Nb-poor melts, rather than the small alkalic melt fractions that Foley (1992) envisages in mantle veins.

3.2.4. Later petrogenesis

Post-subduction high-Nb basalts display chemistries that are consistent with low degree partial mantle melts. High TiO_2, MgO and Fe_2O_3 (Fig. 11) are indicative of mafic compositions, and high trace element contents with a 'flat' pattern and high Nb (Fig. 13) are anticipated in low degree partial melts. This is especially well illustrated in Fig. 15 where samples have much higher Nb/Zr ratios. Low values across Fig. 15 show no source enrichment signatures. Geochemical signals in the high-Nb basalts cannot have been derived from evolution of the same source as previous melts (Gill & Whelan, 1989), leading to the suggestion of gradual migration from the subduction source (Taylor et al., 2000), or emplacement of a new source to the east (Gill & Whelan, 1989).

Moreover, the late-stage dykes at Tuvatu (Fig. 15) show lower ratios which are more similar to late-stage or (non-shoshonitic) post-

subduction rocks.

3.2.5. Model for Fiji

It has long been suggested that shoshonites form as a result of a long, complex history (Arculus and Johnson, 1978), though Fiji is relatively young. The *syn*-subduction arc magmas were formed as a result of flux melting with only minor slab contributions. Polymineralic cumulates formed, with mafic phases including pyroxene and possibly biotite. Residues like this have been observed in Talkeetna and Kohistan (Richards, 2009). Whilst these cumulates contain abundant amphibole, lower water contents and potentially a higher initial Na/K melt chemistry can stabilise biotite rather than amphibole – including as a non-liquidus melt-mineral reaction phase.

It appears that transitional and post-subduction melts were extracted from the same mantle source, a model which is consistent with the previous isotope studies which show a long-lived isotopic character (Gill, 1984; Leslie et al., 2009; Todd et al., 2012). Asthenospheric mantle has been shown to be upwelling beneath Fiji (Hamburger et al., 1988), and potentially allowed decompression melting. There appears to have been a history of mantle metasomatism due to variable slab, fluid, and sediment contributions. Magmas such as post-subduction shoshonites may 'inherit' a subduction component when the same source is later tapped in post-subduction environments. Subcontinental mantle can retain a subduction signature for >40 Ma after subduction cessation (Hole, 1988) and mantle wedges are preserved as heterogeneities for >20 Ma (van Hinsbergen et al., 2020). Yet, this cannot easily explain the switch from transitional magmas to post-subduction shoshonites as they occur in much the same location in a short period of time. This instead points towards a switch in source, to either a distinctly metasomatised part of mantle, or lithospheric cumulates. However, if heterogeneities within the asthenospheric mantle were the source, they must however be a relatively modern characteristic beneath Fiji as this variability is not seen throughout subduction samples. Cumulates more easily allow for small scale heterogeneities.

Overall, extension and some structural control was key to generating magma pathways, and potentially the switch from forming cumulates to disrupting them. True low degree partial melting is unlikely to have occurred until 3 Ma based on Nb—Ta contents. A sudden change of all volcanism in Fiji to 'OIB' composition at occurred at 2.8 Ma (Gill & Whelan, 1989), but is not represented in this dataset.

4. Conclusions

The tectonic history of Fiji is complicated, and this is reflected in the geochemical diversity of magmatic rocks intruded and erupted over a relatively short period of time. Viti Levu's 'Post-subduction' magmatic rocks, including shoshonites, show intense subduction-like signatures (elevated LILE and potassium, depleted HFSE) despite forming in an extensional setting, as the island rotated away from the former Vitiaz arc position.

Integrating newly presented data with pre-existing literature data has shown that although fluxing of fluids and sediment melts from a subducted slab may play a role in producing the distinctive post-subduction magmas, they are likely insufficient to drive the characteristic chemistry of the shoshonites. The same is true of mantle metasomatism during subduction; it cannot fully explain the enrichments of K, Rb and Ba, and depletions of Nb and Ti in the post-subduction suites.

Remelting of cumulates formed during earlier subduction-related magmatism is shown to perhaps play a greater role than has previously been considered. Earlier studies into post-subduction gold mineralisation have suggested cumulates to have a potential role in metallogenic fertility. Lower crustal cumulate piles, formed during the differentiation of *syn*-subduction magmas, represent a potential repository of the elements characteristic of the shoshonites, as well as precious metals. Biotite in particular is a potential source of potassium and LILEs for shoshonites. Remelting and/or assimilation of biotite-

bearing cumulates during extension could liberate both rock forming elements and ore metals to magmas.

Data availability

None.

Declaration of Competing Interest

The authors declare that they have no known competing financial interests or personal relationships that could have appeared to influence the work reported in this paper.

Appendix A. Supplementary data

Supplementary data to this article can be found online at https://doi.org/10.1016/j.lithos.2022.106897.

References

Ahmad, M., 1987. Mineralogical and Geochemical Studies of the Emperor Gold Telluride Deposit, Fiji.

Anderson, R.N., DeLong, S.E., Schwarz, W.M., 1978. Thermal model for subduction with dehydration in the downgoing slab. J. Geol. 86 (6), 731–739. https://doi.org/10.1086/649739.

Anderson, W.B., Eaton, P.C., 1990. Gold mineralisation at the Emperor Mine, Vatukoula, Fiji. J. Geochem. Explor. 36 (1), 267–296. https://doi.org/10.1016/0375-6742(90)90058-I.

Appleton, J.D., 1972. Petrogenesis of Potassium-rich Lavas from the Roccamonfina Volcano, Roman Region, Italy. J. Petrol. 13 (3), 425–456. https://doi.org/10.1093/petrology/13.3.425.

Arculus, R.J., Johnson, R.W., 1978. Criticism of generalised models for the magmatic evolution of arc-trench systems. Earth Planet. Sci. Lett. 39 (1), 118–126. https://doi.org/10.1016/0012-821X(78)90148-6.

Begg, G., Gray, D.R., 2002. Arc dynamics and tectonic history of Fiji based on stress and kinematic analysis of dikes and faults of the Tavua Volcano, Viti Levu Island, Fiji. Tectonics 21 (4), 5–14. https://doi.org/10.1029/2000TC001259.

du Bray, E.A., 2017. Geochemical characteristics of igneous rocks associated with epithermal mineral deposits—a review. Ore Geol. Rev. 80, 767–783.

Bucholz, C., Jagoutz, O., Schmidt, M., Sambuu, O., 2014. Fractional crystallization of high-K arc magmas: biotite- versus amphibole-dominated fractionation series in the Dariv Igneous complex, Western Mongolia. Contrib. Mineral. Petrol. 168 (5), 1–28. https://doi.org/10.1007/s00410-014-1072-9.

Chen, J., Chen, Y.J., Wiens, D.A., Wei, S.S., Zha, Y., Julià, J., Cai, C., 2019. Crustal and lithospheric structure of inactive volcanic arc terrains in Fiji. Tectonophysics 750, 394–403. https://doi.org/10.1016/j.tecto.2018.07.014.

Chen, W., Brudzinski, M.R., 2001. Evidence for a large-scale remnant of subducted lithosphere beneath Fiji. Science 292 (5526), 2475–2479. https://doi.org/10.1126/science.292.5526.2475.

Ciobanu, C.L., Cook, N.J., Spry, P.G., 2006. Preface – Special issue: Telluride and selenide minerals in gold deposits – how and why? Mineral. Petrol. 87 (3), 163–169. https://doi.org/10.1007/s00710-006-0133-9.

Colley, H., Greenbaum, D., 1980. The mineral deposits and metallogenesis of the Fiji Platform. Econ. Geol. 75 (6), 807–829. https://doi.org/10.2113/gsecongeo.75.6.807.

Core, D.P., Kesler, S.E., Essene, E.J., 2006. Unusually Cu-rich magmas associated with giant porphyry copper deposits: evidence from Bingham. Utah Geol. 34 (1), 41–44.

Davidson, J., Turner, S., Handley, H., Macpherson, C., Dosseto, A., 2007. Amphibole "sponge" in arc crust? Geology 35 (9), 787. https://doi.org/10.1130/G23637A.1.

Davidson, J., Turner, S., Plank, T., 2013. Dy/Dy: Variations Arising from Mantle sources and Petrogenetic Processes. J. Petrol. 54 (3), 525–537. https://doi.org/10.1093/petrology/egs076.

Ewart, A., Griffin, W.L., 1994. Application of proton-microprobe data to trace-element partitioning in volcanic rocks. Chem. Geol. 117 (1–4), 251–284.

Foley, S., 1992. Vein-plus-wall-rock melting mechanisms in the lithosphere and the origin of potassic alkaline magmas. Lithos 28 (3), 435–453. https://doi.org/10.1016/0024-4937(92)90018-T.

Forsythe, Nathan A., Spry, Paul G., Thompson, Michael L., 2019. Petrological and Mineralogical Aspects of Epithermal Low-Sulfidation Au-and Porphyry Cu-Style Mineralization, Navilawa Caldera, Fiji. Geosciences 9 (1), 42. https://doi.org/10.3390/geosciences9010042.

Georgiev, S., Marchev, P., Heinrich, C.A., Von Quadt, A., Peytcheva, I., Manetti, P., 2009. Origin of Nepheline-normative High-K Ankaramites and the Evolution of Eastern Srednogorie Arc in SE Europe. J. Petrol. 50 (10), 1899–1933. https://doi.org/10.1093/petrology/egp056.

Gill, J., 1984. Sr Pb Nd isotopic evidence that both MORB and OIB sources contribute to oceanic island arc magmas in Fiji. Earth Planet. Sci. Lett. 68 (3), 443–458. https://doi.org/10.1016/0012-821X(84)90129-8.

Gill, J., Whelan, P., 1989a. Early rifting of an oceanic island arc (Fiji) produced shoshonitic to tholeiitic basalts. J. Geophys. Res. Solid Earth 94 (B4), 4561–4578. https://doi.org/10.1029/JB094iB04p04561.

Gill, J., Whelan, P., 1989b. Postsubduction Ocean island alkali basalts in Fiji. J. Geophys. Res. Solid Earth 94 (B4), 4579–4588. https://doi.org/10.1029/JB094iB04p04579.

Gill, J.B., 1987. Early geochemical evolution of an oceanic island arc and backarc: Fiji and the South Fiji Basin. J. Geol. 95 (5), 589–615. https://doi.org/10.1086/629158.

Grondahl, C., Zajacz, Z., 2017. Magmatic controls on the genesis of porphyry Cu–Mo–au deposits: the Bingham Canyon example. Earth Planet. Sci. Lett. 480, 53–65.

Hamburger, M., Isacks, B., 1988. Diffuse back-arc deformation in the southwestern Pacific. Nature 332 (14).

Hamburger, M.W., Everingham, I.B., Isacks, B.L., Barazangi, M., 1988. Active tectonism within the Fiji platform, Southwest Pacific. Geology 16 (3), 237. ATWTFP>2.3.CO;2.

Harris, N.B.W., Pearce, J.A., Tindle, A.G., 1986. Geochemical characteristics of collision-zone magmatism. Geol. Soc. Spec. Publ. 19 (1), 67–81. https://doi.org/10.1144/GSL.SP.1986.019.01.04.

Hathway, B., 1993. The Nadi Basin: Neogene strike-slip faulting and sedimentation in a fragmented arc, western Viti Levu, Fiji. J. Geol. Soc. 150 (3), 563. https://doi.org/10.1144/gsjgs.150.3.0563.

Hathway, B., 1994. Sedimentation and volcanism in an Oligocene-Miocene intra-oceanic arc and fore-arc, southwestern Viti Levu, Fiji. Geol. Soc. Lond., Spec. Publ. 81 (1), 95. https://doi.org/10.1144/GSL.SP.1994.081.01.06.

Hergt, J.M., Woodhead, J.D., 2007. A critical evaluation of recent models for Lau–Tonga arc–backarc basin magmatic evolution. Chem. Geol. 245 (1), 9–44. https://doi.org/10.1016/j.chemgeo.2007.07.022.

van Hinsbergen, D., Spakman, W., Boorder, H., Dongen, M., Jowitt, S.M., Mason, P.R.D., 2020. Arc-type magmatism due to continental-edge plowing through ancient subduction-enriched mantle. Geophys. Res. Lett. https://doi.org/10.1029/2020GL087484.

Hole, M.J., 1988. Post-subduction alkaline volcanism along the Antarctic Peninsula. J. Geol. Soc. 145 (6), 985–998. https://doi.org/10.1144/gsjgs.145.6.0985.

Holwell, D.A., Fiorentini, M., McDonald, I., Lu, Y., Giuliani, A., Smith, D.J., Keith, M., Locmelis, M., 2019. A metasomatized lithospheric mantle control on the metallogenic signature of post-subduction magmatism. Nat. Commun. 10 (1) https://doi.org/10.1038/s41467-019-11065-4, 3511–10.

Holwell, D.A., Fiorentini, M.L., Knott, T.R., McDonald, I., Blanks, D.E., Campbell McCuaig, T., Gorczyk, W., 2022. Mobilisation of deep crustal sulfide melts as a first order control on upper lithospheric metallogeny. Nat. Commun. 13 (1), 1–12.

Hou, Z., Yang, Z., Lu, Y., Kemp, A., Zheng, Y., Li, Q., Tang, J., Yang, Z., Duan, L., 2015. A genetic linkage between subduction-and collision-related porphyry Cu deposits in continental collision zones. Geology 43 (3), 247–250.

Ionov, D.A., Griffin, W.L., O'Reilly, S.Y., 1997. Volatile-bearing minerals and lithophile trace elements in the upper mantle. Chem. Geol. 141 (3–4), 153–184.

Irvine, T.N., Baragar, W.R.A., 1971. A Guide to the Chemical Classification of the Common Volcanic Rocks. Can. J. Earth Sci. 8 (5), 523–548. https://doi.org/10.1139/e71-055.

Ishikawa, Y., Sawaguchi, T., Iwaya, S., Horiuchi, M., 1976. Delineation of prospecting targets for Kuroko deposits based on modes of volcanism of underlying dacite and alteration halo. Min. Geol. 26, 105–117.

Jagoutz, O., Müntener, O., Schmidt, M.W., Burg, J., 2011. The roles of flux- and decompression melting and their respective fractionation lines for continental crust formation: evidence from the Kohistan arc. Earth Planet. Sci. Lett. 303 (1), 25–36. https://doi.org/10.1016/j.epsl.2010.12.017.

Jensen, E.P., Barton, M.D., 2000. Gold deposits related to alkaline magmatism. SEG Rev. 13, 279–314.

Kelley, K.D., Ludington, S., 2002. Cripple Creek and other alkaline-related gold deposits in the southern Rocky Mountains, USA: influence of regional tectonics. Mineral. Deposita 37 (1), 38–60.

Kelley, K.D., Spry, P.G., 2016. Critical elements in alkaline igneous rock-related epithermal gold deposit. Rev. Econ. Geol. 18, 195–216.

Large, R.R., 2001. The alteration box plot: a simple approach to understanding the relationship between alteration mineralogy and lithogeochemistry associated with volcanic-hosted massive sulfide deposits. Econ. Geol. Bull. Soc. Econ. Geol. 96 (5), 957–971. https://doi.org/10.2113/96.5.957.

Lee, C.A., Tang, M., 2020. How to make porphyry copper deposits. Earth Planet. Sci. Lett. 529, 115868.

Leslie, R.A.J., Danyushevsky, L.V., Crawford, A.J., Verbeeten, A.C., 2009. Primitive shoshonites from Fiji: Geochemistry and source components. Geochem. Geophys. Geosyst. 10 (7), n/a. https://doi.org/10.1029/2008GC002326.

Mathieu, L., 2018. Quantifying hydrothermal alteration: a review of methods. Geosciences (Basel) 8 (7), 245. https://doi.org/10.3390/geosciences8070245.

Medard, E., Schmidt, M.W., Schiano, P., Ottolini, L., 2006. Melting of amphibole-bearing wehrlites: an experimental study on the origin of ultra-calcic nepheline-normative melts. J. Petrol. 47 (3), 481–504. https://doi.org/10.1093/petrology/egi083.

Moyen, J., 2009. High Sr/Y and La/Yb ratios: the meaning of the "adakitic signature". Lithos 112 (3), 556–574. https://doi.org/10.1016/j.lithos.2009.04.001.

Müller, D., Groves, D.I., Heithersay, P.S., 1994. The shoshonite porphyry Cu-Au association in the Goonumbla district, NSW, Australia. Mineral. Petrol. 51 (2), 299–321.

Pals, D.W., Spry, P.G., 2003. Telluride mineralogy of the low-sulfidation epithermal Emperor gold deposit, Vatukoula, Fiji. Mineral. Petrol. 79 (3), 285–307. https://doi.org/10.1007/s00710-003-0013-5.

Petterson, M.G., Babbs, T., Neal, C.R., Mahoney, J.J., Saunders, A.D., Duncan, R.A., Tolia, D., Magu, R., Qopoto, C., Mahoa, H., Natogga, D., 1999. Geological–tectonic framework of Solomon Islands, SW Pacific: crustal accretion and growth within an intra-oceanic setting. Tectonophysics 301 (1), 35–60. https://doi.org/10.1016/S0040-1951(98)00214-5.

Plank, T., Langmuir, C.H., 1998. The chemical composition of subducting sediment and its consequences for the crust and mantle. Chem. Geol. 145 (3), 325–394. https://doi.org/10.1016/S0009-2541(97)00150-2.

Rahiman, T.I.H., Pettinga, J.R., 2008. Analysis of lineaments and their relationship to Neogene fracturing, SE Viti Levu, Fiji. GSA Bull. 120 (11–12), 1544–1555. https://doi.org/10.1130/B26264.1.

Reubi, O., Blundy, J., 2008. Assimilation of plutonic roots, formation of high-K 'exotic'melt inclusions and genesis of andesitic magmas at Volcán de Colima, Mexico. J. Petrol. 49 (12), 2221–2243.

Richards, J., 2009. Postsubduction porphyry Cu-au and epithermal au deposits: Products of remelting of subduction-modified lithosphere. Geology 37 (3), 247–250. https://doi.org/10.1130/G25451A.1.

Richards, J., 2011. Magmatic to hydrothermal metal fluxes in convergent and collided margins. Ore Geol. Rev. 40 (1), 1–26. https://doi.org/10.1016/j.oregeorev.2011.05.006.

Richards, J.P., Chappell, B.W., McCulloch, M.T., 1990. Intraplate-type magmatism in a continent-island-arc collision zone: Porgera intrusive complex, Papua New Guinea. Geology 18 (10), 958–961.

Rodda, P., 1967. Outline of the geology of Viti Levu. N. Z. J. Geol. Geophys. 10 (5), 1260–1273. https://doi.org/10.1080/00288306.1967.10420217.

Rogers, N.W., Setterfield, T.N., 1994. Potassium and incompatible-element enrichment in shoshonitic lavas from the Tavua volcano, Fiji. Chem. Geol. 118 (1), 43–62. https://doi.org/10.1016/0009-2541(94)90169-4.

Ronacher, E., Richards, J.P., Reed, M.H., Bray, C.J., Spooner, E., Adams, P.D., 2004. Characteristics and evolution of the hydrothermal fluid in the North zone high-grade area, Porgera gold deposit, Papua New Guinea. Econ. Geol. 99 (5), 843–867.

Saunders, A., Rogers, G., Marriner, G.F., Terrell, D.J., Verma, S.P., 1987. Geochemistry of Cenezoic volcanic rocks, Baja California, Mexico: implications for the petrogenesis of post-subduction magmas. J. Volcanol. Geotherm. Res. 32 (1), 223–245. https://doi.org/10.1016/0377-0273(87)90046-1.

Scherbarth, N.L., Spry, P.G., 2006. Mineralogical, petrological, stable isotope, and fluid inclusion characteristics of the Tuvatu Gold-Silver Telluride deposit, Fiji: comparisons with the emperor deposit. Econ. Geol. 101 (1), 135–158. https://doi.org/10.2113/gsecongeo.101.1.135.

Schiano, P., Eiler, J.M., Hutcheon, I.D., Stolper, E.M., 2000. Primitive CaO-rich, silica-undersaturated melts in island arcs: evidence for the involvement of clinopyroxene-rich lithologies in the petrogenesis of arc magmas. Geochem. Geophys. Geosyst. 1 (1) https://doi.org/10.1029/1999GC000032.

Schmidt, M.W., Jagoutz, O., 2017. The global systematics of primitive arc melts. Geochem. Geophys. Geosyst. 18 (8), 2817–2854. https://doi.org/10.1002/2016GC006699.

Schmidt, M.W., Vielzeuf, D., Auzanneau, E., 2004. Melting and dissolution of subducting crust at high pressures: the key role of white mica. Earth Planet. Sci. Lett. 228 (1–2), 65–84. https://doi.org/10.1016/j.epsl.2004.09.020.

Schmitt, Axel K., Stockli, Daniel F., Hausback, Brian P., 2006. Eruption and magma crystallization ages of Las Tres Vírgenes (Baja California) constrained by combined 230Th/238U and (U–Th)/He dating of zircon. J. Volcanol. Geotherm. Res. 158 (3–4), 281–295.

Setterfield, T.N., Mussett, A.E., Oglethorpe, R., 1992. Magmatism and associated hydrothermal activity during the evolution of the Tavua Caldera; 40 Ar-39 Ar dating of the volcanic, intrusive, and hydrothermal events. Econ. Geol. 87 (4), 1130–1140.

Sillitoe, R.H., 1997. Characteristics and controls of the largest porphyry copper-gold and epithermal gold deposits in the circum-Pacific region. Aust. J. Earth Sci. 44 (3), 373–388. https://doi.org/10.1080/08120099708728318.

Sillitoe, R.H., 2002. Some metallogenic features of gold and copper deposits related to alkaline rocks and consequences for exploration. Mineral. Deposita 37 (1), 4–13. https://doi.org/10.1007/s00126-001-0227-6.

Smith, D.J., 2014. Clinopyroxene precursors to amphibole sponge in arc crust. Nat. Commun. 5 (1), 1–6.

Smith, D.J., Naden, J., Jenkin, G.R.T., Keith, M., 2017. Hydrothermal alteration and fluid pH in alkaline-hosted epithermal systems. Ore Geol. Rev. 89, 772–779. https://doi.org/10.1016/j.oregeorev.2017.06.028.

Sorbadere, F., Schiano, P., Métrich, N., 2013. Constraints on the origin of nepheline-normative primitive magmas in island arcs inferred from olivine-hosted melt inclusion compositions. J. Petrol. 54 (2), 215–233. https://doi.org/10.1093/petrology/egs063.

Stratford, J.M.C., Rodda, P., 2000. Late miocene to pliocene palaeogeography of Viti Levu, Fiji Islands. Palaeogeogr. Palaeoclimatol. Palaeoecol. 162 (1), 137–153. https://doi.org/10.1016/S0031-0182(00)00109-7.

Taylor, G., Gascoyne, J., Colley, H., 2000. Rapid rotationof Fiji: paleomagnetic evidence and tectonic implications. J. Geophys. Res. 105, 5771–5781.

Taylor, W.R., Rock, N.M.S., Groves, D.I., Perring, C.S., Golding, S.D., 1994. Geochemistry of Archean shoshonitic lamprophyres from the Yilgarn Block, Western Australia: au abundance and association with gold mineralization. Appl. Geochem. 9 (2), 197–222. https://doi.org/10.1016/0883-2927(94)90007-8.

Todd, E., Gill, J.B., Pearce, J.A., 2012. A variably enriched mantle wedge and contrasting melt types during arc stages following subduction initiation in Fiji and Tonga, Southwest Pacific. Earth Planet. Sci. Lett. 335-336, 180–194. https://doi.org/10.1016/j.epsl.2012.05.006.

Turner, S., Foden, J., George, R., Evans, P., Varne, R., Elburg, M., Jenner, G., 2003. Rates and processes of potassic magma evolution beneath Sangeang Api Volcano, East Sunda Arc, Indonesia. J. Petrol. 44 (3), 491–515. https://doi.org/10.1093/petrology/44.3.491.

Villement, B., Jaffrezic, H., Joron, J., Treuil, M., 1981. Distribution coefficients of major and trace elements; fractional crystallization in the alkali basalt series of Cahine des Puys (Massif Central, France). Geochim. Cosmochim. 45, 1997–2016.

Wharton, M.R., Hathway, B., Colley, H., 1995. Volcanism associated with extension in an Oligocene–Miocene arc, southwestern Viti Levu, Fiji. Geol. Soc. Lond., Spec. Publ. 81 (1), 95. https://doi.org/10.1144/GSL.SP.1994.081.01.06.

Whelan, P.M., Gill, J.B., Kollman, E., Duncan, R.A., Drake, R.E., 1985. Radiometric dating of magmatic stages in Fiji.

Wolfe, R.C., Cooke, D.R., 2011. Geology of the Didipio region and genesis of the Dinkidi alkalic porphyry Cu-au deposit and related pegmatites, northern Luzon, Philippines. Econ. Geol. 106 (8), 1279–1315.

Zanetti, A., Mazzucchelli, M., Rivalenti, G., Vannucci, R., 1999. The Finero phlogopite-peridotite massif: an example of subduction-related metasomatism. Contrib. Mineral. Petrol. 134 (2), 107–122. https://doi.org/10.1007/s004100050472.